

Far UV and Optical Emissions from Three Apparent Supernova Remnants Located at Unusually High Galactic Latitudes

ROBERT A. FESEN,¹ MARCEL DRECHSLER,² KATHRYN E. WEIL,³ XAVIER STROTTNER,⁴ JOHN C. RAYMOND,⁵
DAN MILISAVLJEVIC,³ BHAGYA M. SUBRAYAN,³ DENNIS DI CICCIO,⁶ SEAN WALKER,⁶ AND DAVID MITTELMAN⁶

¹6127 Wilder Lab, Department of Physics and Astronomy, Dartmouth College, Hanover, NH 03755 USA

²Baarenstein Observatory, Feldstrasse 17, D-09471 Baarenstein, Germany

³Department of Physics and Astronomy, Purdue University, 525 Northwestern Avenue, West Lafayette, IN 47907 USA

⁴Montfrazee, 01370 Saint Etienne Du Bois France

⁵Harvard-Smithsonian Center for Astrophysics, 60 Garden St., Cambridge, MA 02138, USA

⁶MDW Sky Survey, New Mexico Skies Observatory, Mayhill, NM 88339, USA

ABSTRACT

Galactic supernova remnants (SNRs) with angular dimensions greater than a few degrees are relatively rare, as are remnants located more than ten degrees off the Galactic plane. Here we report the results of a UV and optical investigation of two previously suspected SNRs that are more than $\simeq 10$ degrees in both angular diameter and Galactic latitude. One is the proposed G354-33 remnant discovered in 2008 through 1420 MHz polarization maps. GALEX far UV (FUV) emission and H α mosaics show the object's radio emission coincident with a nearly continuous $11^\circ \times 14^\circ$ shell of thin UV filaments which surround a broad H α emission ring. Another proposed high latitude SNR is the enormous $20^\circ \times 26^\circ$ Antlia nebula (G275.5+18.4) discovered in 2002 through low-resolution all-sky H α images and ROSAT soft X-ray emission. GALEX FUV image mosaics along with deep H α images and optical spectra of several filaments indicate the presence of shocks throughout the nebula with estimated shock velocities of 70 to over 100 km s⁻¹. We conclude that both of these nebulae are bona fide SNRs with estimated ages less than 10^5 yr despite their unusually large angular dimensions. Using FUV and optical spectra and images, we also report finding an apparent new, high latitude SNR (G249.2+24.4) approximately $2.8^\circ \times 4.2^\circ$ in size based on its UV and optical emission properties.

Keywords: SN: individual objects: ISM: supernova remnant

1. INTRODUCTION

In spite of an increasing variety of supernovae (SNe) sub-types, the majority of SNe are generally believed to release $0.5 - 2 \times 10^{51}$ erg, although superluminous SNe may release substantially more (Howell 2017). Only a small percentage of this comes out as visible light, with most of a SN's energy initially carried away in the form of kinetic energy. It is this enormous point deposition of energy that has a significant impact on the structure and energy content of a galaxy's interstellar medium through an expanding remnant that can last largely intact up to $\simeq 10^5$ yr (Cox & Smith 1974; McKee & Ostriker 1977; Blondin et al. 1998).

Currently, there are some 300 confirmed Galactic supernova remnants (SNRs) catalogued with dozens of other suspected SNRs and more added every few years (Ferrand & Safi-Harb 2012; Green 2019). Most Galactic SNRs are less than a degree in angular size, more than 1 kpc distant and well evolved, with typical estimated ages between 10^4 and 10^5 yr.

Out-sized attention relative to their population percentage has been directed to the handful of the Milky

Way's young remnants with ages less than 5000 yr. These include the Crab Nebula, Cassiopeia A, the remnants of Tycho and Kepler, the Vela remnant, and Puppis A. This increased attention is due to their high expansion velocities, metal-rich ejecta, bright emission across the entire electromagnetic spectrum, and clearer connections to the various core-collapse and thermonuclear SN sub-types.

The majority of Galactic SNRs were first detected through radio observations due to their characteristic synchrotron nonthermal radio emission associated with shocked gas (Downes 1971; Chevalier 1977; Green 1984, 2004). Such nonthermal emission leads to a power law flux density, S , with $S \propto \nu^{-\alpha}$ where α is the emission spectral index with typical SNR values between -0.3 and -0.7. Rarer pulsar wind-driven SNRs exhibit a much flatter radio spectrum, with spectral indices around zero.

While multi-frequency radio surveys have been historically the dominant tool for finding SNRs, X-ray studies have also led to the discovery of several additional SNRs. These include RX J1713.7-3946 (G347.3-0.5; Pfeffermann & Aschenbach 1996) and the young "Vela Junior" SNR (G266.2-1.2; Aschenbach 1998) coincident with the

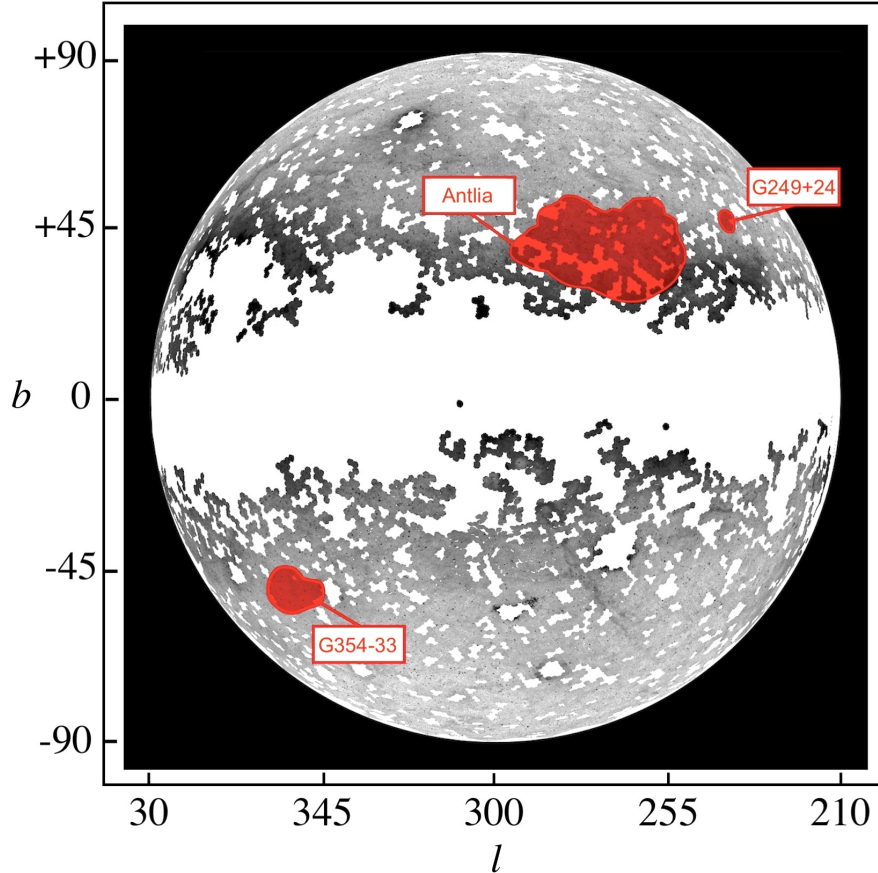


Figure 1. GALEX FUV intensity map of half of the sky in Galactic coordinates, showing locations of two apparent SNRs, G249+24 and G354-33, and the exceptionally large Antlia SNR. White areas denote regions with no GALEX imaging data.

much larger Vela SNR. Recent examples of X-ray confirmed or discovered remnants include several new SNRs in the LMC (Maggi et al. 2014) and X-ray confirmation of the suspected Galactic remnant G53.4+0.0 (Driessen et al. 2018).

Despite the fact that less than 50% of Galactic SNRs exhibit any appreciable associated optical emission, a remnant’s optical emission can be useful in confirming the presence of high-velocity shocks and in defining a remnant’s overall size and morphology. Although discoveries of new SNRs in the optical is relatively rare, there have been several recently reported discoveries (Stupar et al. 2007; Boumis et al. 2009; Stupar & Parker 2012; Fesen et al. 2015; Neustadt et al. 2017; Stupar et al. 2018; How et al. 2018; Fesen et al. 2019) along with many proposed SNR candidates (Stupar et al. 2008; Stupar & Parker 2011; Boumis et al. 2009; Alikakos et al. 2012; Sabin et al. 2013).

The main criterion for optical SNR identification is a line ratio of $I([\text{S II}])/I(\text{H}\alpha) \geq 0.4$ which has proven useful in identifying the shocked emission of SNRs in both the Milky Way and nearby local group galaxies (Blair et al. 1981; Dopita et al. 1984; Fesen et al. 1985; Leonidaki et al. 2013; Long 2017). Recently, the near

infrared $[\text{Fe II}]$ line emissions at 1.27 and 1.64 μm have also been used to detect dust obscured SNRs in nearby galaxies (see review by Long 2017).

One wavelength regime that has not yet been fully exploited to search for new Galactic SNRs is the ultra-violet (UV). Here we present results of an initial study of SNRs located far away from the Galactic plane using wide field-of-view (FOV) UV images assembled from the Galaxy Evolution Explorer (GALEX) All-Sky survey (Bianchi 2009). We began this research by investigating two unusually high latitude suspected supernova remnants including the exceptionally large Antlia remnant (McCullough et al. 2002). During this work, we also found a new apparent SNR. UV and optical images plus some follow-up optical spectra are described in §2, with results presented in §3. We discuss the general properties of these SNRs in §4, with our conclusions and discussion of helpful follow-up observations given in §5.

2. DATA AND OBSERVATIONS

2.1. GALEX UV Images

The GALEX satellite was a NASA science mission led by the California Institute of Technology who operated

Table 1. Locations and Dimensions of SNRs

SNR ID	Approximate Center (J2000)	Galactic Coordinates	Diameter	Distance for Dia. = 100 pc
G354-33	RA = 20 ^h 16 ^m Dec = −46°00′	$l = 353.9$ $b = -33.4$	$11^\circ \times 14^\circ$	~500 pc
G249+24	RA = 09 ^h 31 ^m Dec = −16°40′	$l = 249.2$ $b = +24.4$	$2.8^\circ \times 4.2^\circ$	~1500 pc
Antlia	RA = 10 ^h 38 ^m Dec = −37°20′	$l = 275.5$ $b = +18.4$	$20^\circ \times 26^\circ$	~250 pc

it from July 2003 through February 2012. The main instrument was a 50 cm diameter modified Ritchey-Chrétien telescope, a dichroic beam splitter and astigmatism corrector, and two microchannel plate detectors to simultaneously cover two wavelength bands with a 1.25 degree field of view with a resolution of $1.5'' \text{ pixel}^{-1}$. Direct images were obtained in two broad bandpasses: a far-UV (FUV) channel sensitive to light in the 1344 to 1786 Å range, and a near-UV (NUV) channel covering 1771 to 2831 Å. Resulting images are circular in shape with an image FWHM resolution of $\sim 4.2''$ and $\sim 5.3''$ in the FUV and NUV bands, respectively.

Being mainly a mission to study the UV properties of galaxies in the local universe, GALEX survey images largely avoided the complex and external galaxy poor Galactic plane. However, even its All-Sky Survey program focused away from the plane of the Milky Way did not cover all possible areas, leading to numerous gaps (see Fig. 1). Nonetheless, some 26,000 square degrees were imaged to a depth of $m_{AB} = 20.5$ (Bianchi 2009). Using the on-line GALEX images, large FUV and NUV image mosaics were examined of several regions typically more than 10 degrees off the Galactic plane.

2.2. $H\alpha$ images

Wide-field, low-resolution $H\alpha$ images of regions around suspected SNRs obtained as part of the MDW Hydrogen-Alpha Survey¹ were examined. This survey uses a 130 mm telescope at the New Mexico Skies Observatory, with a FLI ProLine 16803 CCD and 3 nm filter centered on $H\alpha$. This telescope-camera system has a field-of-view (FOV) of approximately $3^\circ 5' \times 3^\circ 5'$ with a pixel size of $3''.17$. Each field was observed 12 times each with an exposure of 1200 s.

Follow-up, higher-resolution images of interesting FUV filaments were obtained with a 1.3m telescope at the MDM Observatory at Kitt Peak, Arizona using a 1024×1024 pixel CCD yielding a FOV of $8.5'$. With on-chip 2×2 pixel binning, spatial resolution was $1.05''$. Two exposures of 900 s each were taken at four positions where the FUV images of G249+24 exhibited optical filaments and where long slit spectra were also obtained.

We have also made large mosaics from Southern $H\alpha$ Sky Survey Atlas (SHASSA; Gaustad et al. 2001). This

wide-angle robotic survey covered $\delta = +15^\circ$ to -90° with 13° square images with an angular resolution of $\simeq 0.8'$. Narrow passband continuum filters on blue and red sides of $H\alpha$ centered at 6440 and 6770 Å allow for stellar and background subtraction. The survey had a native sensitive level of $1.2 \times 10^{-17} \text{ erg cm}^{-2} \text{ s}^{-1} \text{ arcsec}^{-2}$ which could be significantly lowered with smoothing.

2.3. Optical Spectra

Low-dispersion optical spectra of filaments in the more northern suspected SNR were obtained with the MDM 2.4m Hiltner telescope using Ohio State Multi-Object Spectrograph (OSMOS; Martini et al. 2011). Employing a blue VPH grism ($R = 1600$) and a 1.2 arcsec wide slit, exposures of 2×900 s were taken covering 4000–6900 Å with a spectral resolution of 1.2 Å pixel^{-1} and a FWHM = 3.5 Å. Spectra were extracted from regions clean of appreciable emission along each of the 15 arcminute slits.

For southern hemisphere nebulae, spectra were taken of suspected SNR filaments using the Robert Stobie Spectrograph (RSS) on the 10 m SALT telescope in South Africa. Using a 900 lines per mm and a 1.5 arcsec wide slit, spectra were obtained covering 4050 to 7120 Å region with a FWHM resolution of 5 Å and a dispersion of 1.0 Å pix^{-1} . Exposures ranged from 2×300 s to 2×600 s.

SALT spectra were reduced using SALT reduction software while MDM images and spectra were reduced using the OSMOS reduction pipelines² in Astropy. MDM spectra were further reduced using PYRAF³ and L.A. Cosmic (van Dokkum 2001) to remove cosmic rays and calibrated using a HgNe or Ar lamp and spectroscopic standard stars (Oke 1974; Massey & Gronwall 1990).

3. RESULTS

A few large and unusually high Galactic latitude nebulae have been recently proposed as previously unrecognized SNRs. These objects have angular diameters well in excess of the largest confirmed SNRs, namely the 8° diameter Vela SNR. If these objects were to be found to be true SNRs, they would help expand the notion of

¹ <https://www.mdwskysurvey.org>

² <https://github.com/jrthorstensen/thorosmos>

³ PYRAF is a product of the Space Telescope Science Institute, which is operated by AURA for NASA.

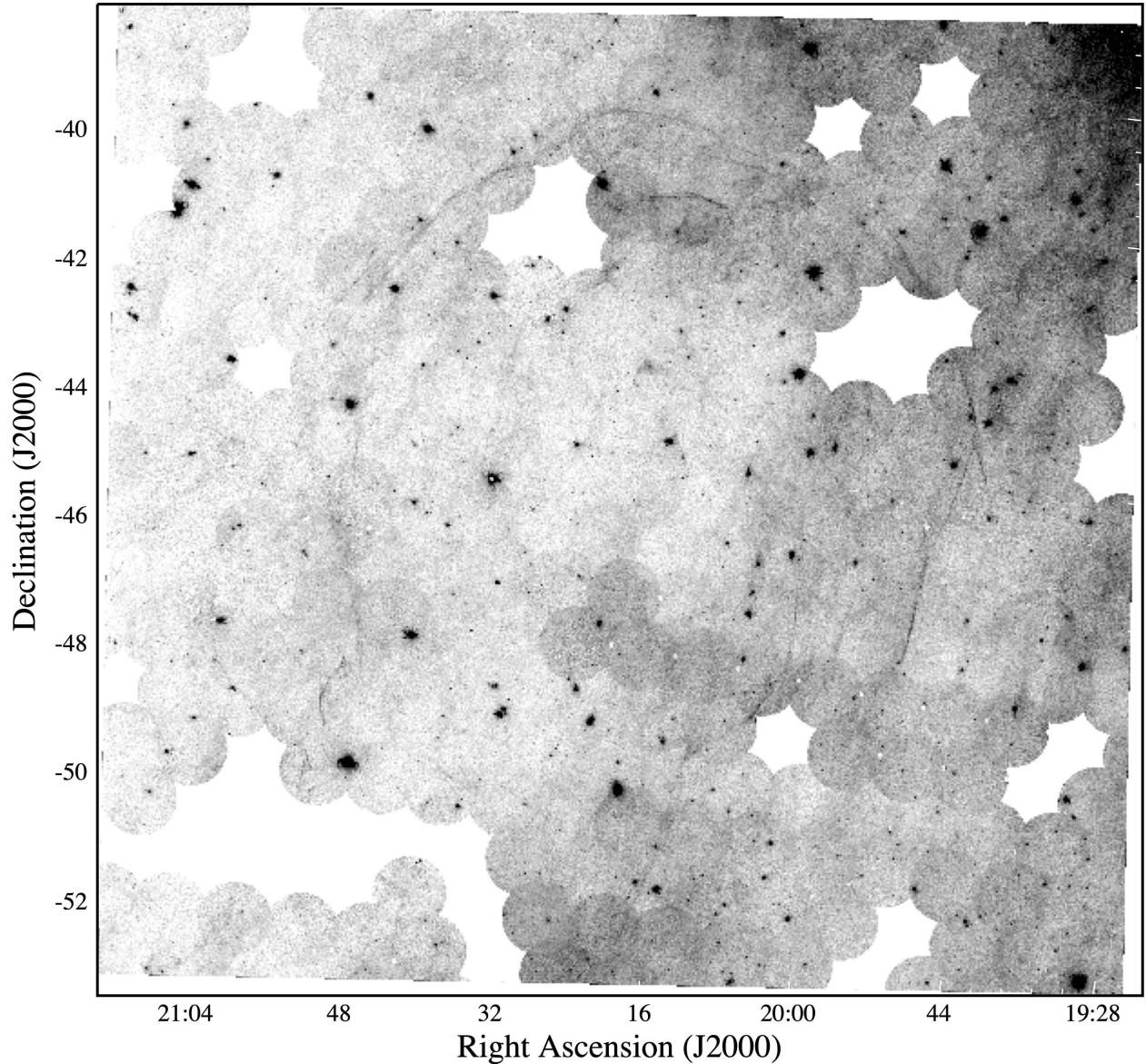


Figure 2. GALEX FUV intensity map of G354-33 showing a roughly spherical shell of UV emission filaments. Approximate shell center: $20^{\text{h}} 16.0^{\text{m}} 36^{\text{s}} -45^{\circ} 40'$. Note: Individual circular GALEX images are 1.2° in diameter.

how large an identifiable remnant can be and how far off the plane should SNR researchers be looking.

The proposed new SNRs include the huge $\sim 24^{\circ}$ diameter Antlia nebula (G275.5+18.4; [McCullough et al. 2002](#)) and the $\sim 10^{\circ}$ diameter radio remnant G354-33 ([Testori et al. 2008](#)). Due to limited data on it, Antlia is listed only as a possible SNR in the most recent catalogue of Galactic supernova remnants ([Green 2019](#)), whereas no mention is made of G354-33 in either this 2019 SNR catalogue or in online SNR lists⁴. Below

we discuss GALEX far UV (FUV) and optical properties of these two suspected SNRs, plus a third object, G249.2+24.4, which we believe is likely a new SNR. The presentation order follows that of our research work.

3.1. *The Suspected Radio SNR G354-33*

Using a 1420 MHz linear polarization survey of the southern hemisphere sky, [Testori et al. \(2008\)](#) identified a large $\sim 10^{\circ}$ depolarized shell at $\alpha(\text{J2000}) = 20^{\text{h}} 25^{\text{m}}$, $\delta(\text{J2000}) = -47^{\circ}$, roughly corresponding to Galactic coordinates $l = 353^{\circ}$ $b = -34^{\circ}$. This shell could also be seen in a 1.4 GHz polarization all-sky survey map ([Reich & Reich 2009](#)). Due to the object's spherical morphology and radio properties, [Testori et al. \(2008\)](#) suggested a SNR identification, with a size suggesting a distance

⁴ <http://www.mrao.cam.ac.uk/surveys/snrs/snrs.info.html>
<http://snrcat.physics.umanitoba.ca/index.php?>

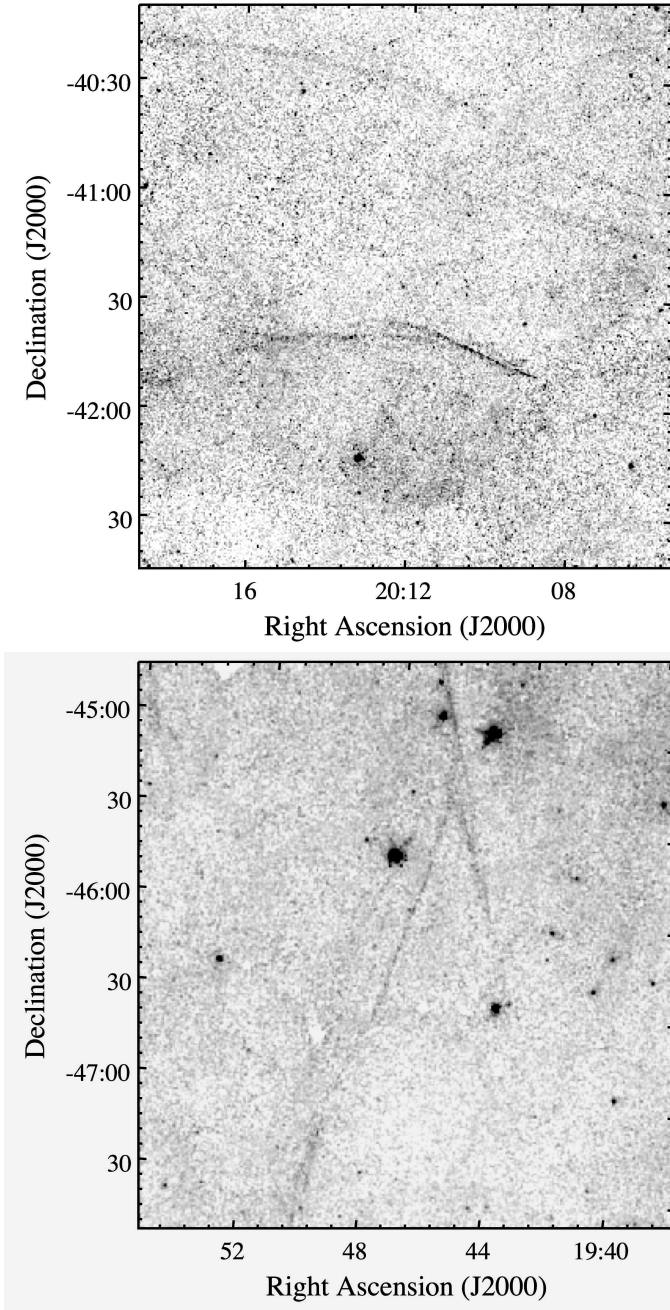


Figure 3. **Top:** Blow-up of a small section of the GALEX FUV map of G354-33 along the remnant’s northern rim. **Bottom:** Blow-up of a small section along G354-33’s western limb.

between 300 and 500 pc, a physical diameter of $17.4 \text{ pc} \times d_{100\text{pc}}$ and a z distance of $57.4 \text{ pc} \times d_{100\text{pc}}$. Testori et al. (2008) noted that the object could be seen in 408 MHz data (Haslam et al. 1982) and weakly in the SHASSA $H\alpha$ images (Gaustad et al. 2001). This object also shows up in gradients of linearly polarized synchrotron radio emission (Iacobelli et al. 2014).

Recently, Bracco et al. (2020) briefly commented on the presence of some GALEX FUV filaments coincident with this radio shell. However, to our knowledge, there is no paper showing this suspected SNR’s FUV emissions. Below we present large mosaics of GALEX FUV images along with a SHASSA $H\alpha$ image and compare these to the low resolution 1420 MHz radio images.

3.1.1. Far UV and $H\alpha$ Images

Wide-field mosaics of GALEX far UV (FUV) and near UV (NUV) images show a large, faint UV emission shell largely coincident with the 1420 MHz radio shell. The UV emission consists of over a dozen thin emission filaments. Because these filaments appear brightest in the GALEX FUV images compared to NUV images, we will concentrate mainly on the shell’s far UV emission structure.

The strong shock-like morphology of these filaments and their arrangement in a nearly continuous shell lends support to Testori et al. (2008)’s suggestion for it to be a previously unrecognized Galactic supernova remnant, albeit with unusually large angular dimensions and distance from the Galactic plane.

Figure 2 shows a mosaic of GALEX FUV images of G354-34 smoothed by a nine point Gaussian⁵. As seen in this FUV mosaic, the object exhibits a large and coherent set of sharp UV emitting filaments arranged in a nearly complete shell-like structure. Multiple and overlapping filaments are common along the northern and western limbs. Although many filaments are unresolved at GALEX’s $4.6''$ FWHM resolution, some filaments appear partially resolved in places, especially along its northernmost edge. It is not clear if this appearance is due to closely spaced multiple filaments or resolution of a single emission filament.

Based on its brighter FUV filaments, we estimate somewhat larger angular dimensions than the 10° cited by Testori et al. (2008). Instead, we find dimensions of $\simeq 11^\circ$ East-West and $\simeq 14^\circ$ North-South, with a distinct indentation along its south-western limb. Its southern extent is poorly constrained in our GALEX FUV mosaic but FUV filaments extend south to at least a Declination of -53° .

Due to its large size, many of the filamentary details visible in the full resolution FUV mosaic are lost in Figure 2. Consequently, we show in Figure 3 blow-ups of two regions, one along G354-33’s northern rim and one along its western limb to give a better sense of its fine-scale morphology. It should be noted that some individual filaments are two to three degrees in length, equivalent to the entire lengths of some of the largest Galactic SNRs.

⁵ Because of distortions due to the large size of this emission structure, coordinates shown are only accurate to a few arc minutes.

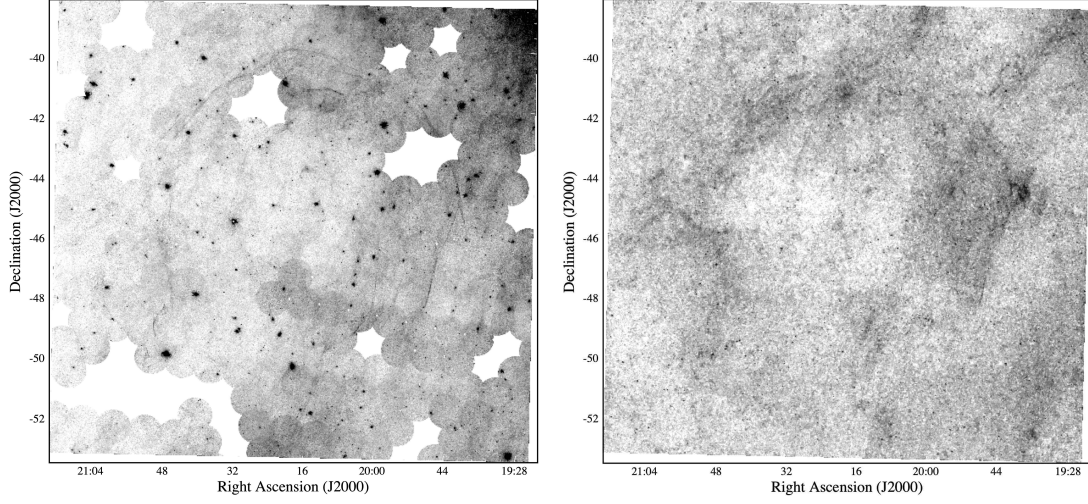


Figure 4. GALEX FUV (left) and continuum subtracted SHASSA $H\alpha$ (right) images of G354-33.

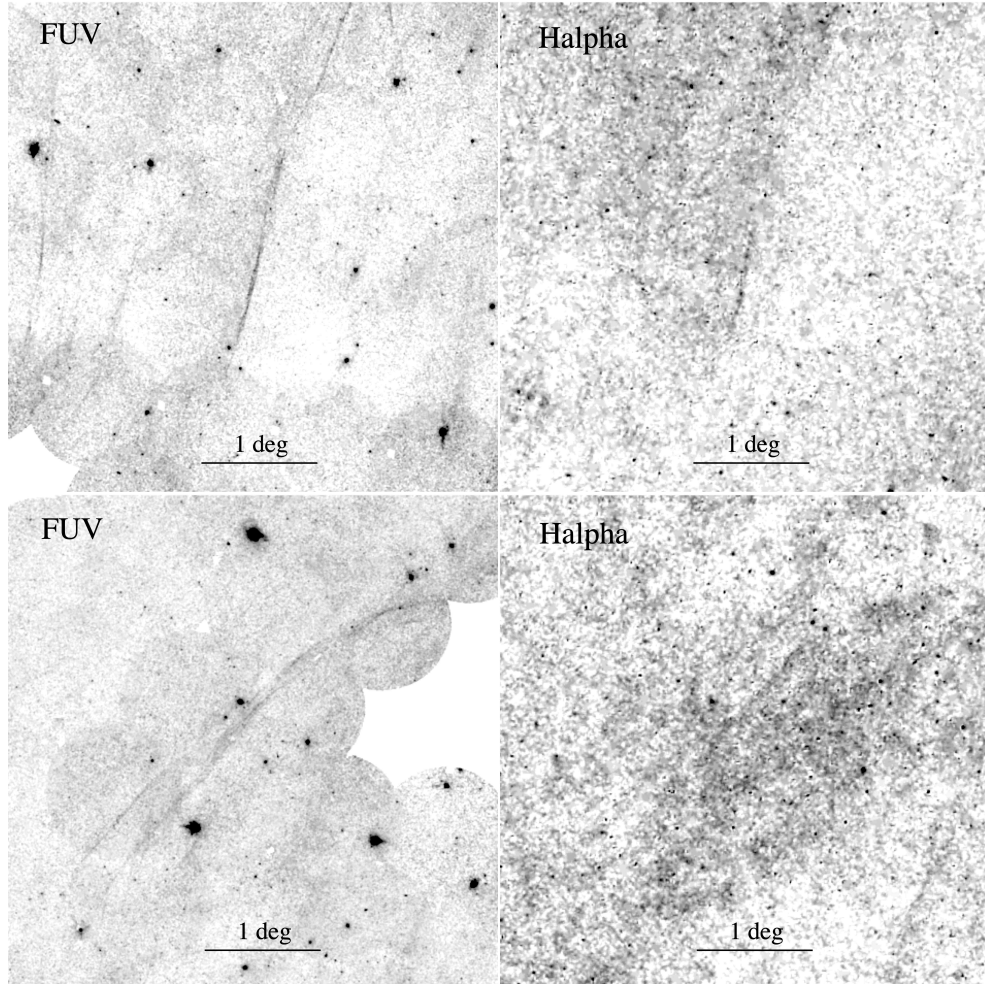


Figure 5. Matched GALEX FUV and SHASSA $H\alpha$ images for a bright filament along G354-33's western limb (upper panels) and northeastern limb (lower panels). Field centers are: $20^{\text{h}} 34.0^{\text{m}} -42^{\circ}15'$ (top) and $19^{\text{h}} 50.1^{\text{m}} -47^{\circ}52'$ (bottom).

Continuum subtracted SHASSA $H\alpha$ image mosaics of the remnant region reveal a large and thick diffuse shell of emission located within the boundaries of the FUV filaments. Figure 4 shows the GALEX FUV along side of the SHASSA $H\alpha$ image covering the same sky region. The $H\alpha$ emission structure is far more diffuse than that seen in the GALEX FUV image with very few filaments. We estimate an $H\alpha$ flux of around $1-2 \times 10^{-17}$ erg cm $^{-2}$ s $^{-1}$ arcsec $^{-2}$ for most of the diffuse emission and about 3 times times this for the area of brighter emission along the nebula’s northwestern limb.

While its $H\alpha$ emission’s location matches that seen in the FUV image, weak $H\alpha$ emission is seen to extend farther to the east and south than is readily visible in the GALEX FUV mosaic image. However in general, the FUV filaments appear to mark the outer edges of the diffuse $H\alpha$ emission shell.

This is shown in Figure 5 where we compare FUV vs. $H\alpha$ images for western and northeastern sections along its limb. The upper images show the presence of weak $H\alpha$ emission coincident with the bright main section of the FUV filament, with diffuse $H\alpha$ emission extending toward the east bordered by the long FUV filament. The lower panels show a section along the nebula’s northeastern limb where again the UV filaments are seen to mark the extent of the diffuse $H\alpha$ emission. The SHASSA image also gives a hint of filamentary structure that resembles that seen in the FUV image.

3.1.2. Radio and X-rays

As already noted, Testori et al. (2008) used the 1420 MHz Villa Elisa radio data (Testori et al. 2001) to identify the radio emission ring, G354-33, as a possible SNR. The upper panel of Figure 6 shows a $60^\circ \times 25^\circ$ wide section of the Villa Elisa 1420 MHz polarization southern sky survey data roughly centered on the remnant. The emission ring appears distinct in shape and separate from other emission features along the southern edge of the Galactic plane (i.e., the right-hand side of the image).

The images in the lower panel of Figure 6 show identical regions of a GALEX FUV image mosaic (left panel) and the 1420 MHz Villa Elisa radio image (right panel). Overall, there is good agreement in both size and location for the FUV emission shell and radio ring seen in these images. This includes the greater extent toward the southern limb area. We note that the brightest portion of this radio emission shell lies on the object’s western limb, the side facing the Galactic plane.

While coincident in location, the radio shell has a smaller diameter of $\simeq 10^\circ$ than the roughly 11° East-West diameter seen in the FUV images and is centered around $20^h 19^m 47^s - 46^\circ 25'$ ($l=353.5$ $b=-34.2$) which is slightly different from that of the GALEX FUV emission shell (see Table 1). Thus, although we have used the name G354-33 above following Testori et al. (2008),

we believe the object’s correct Galactic coordinate name should be G353.9-33.4 (see Table 1).

Examination of ROSAT on-line data showed no obvious associated X-ray emission with this nebula. This is not surprising given its location 33.4° below the Galactic plane. Moreover, in view of the lack of any bright FUV emission nebulae along its limbs, this suggests that it lies in a region with few or none large-scale interstellar clouds which might generate significant X-ray flux.

3.2. G249.2+24.4

Using GALEX FUV mosaics, we discovered a region containing several long, thin, shock-like morphology filaments aligned mostly N-S and arranged in a roughly elliptical shape $\sim 2.5 \times 4^\circ$ in size. These filaments appear centered at $\alpha(\text{J2000}) = 9^h 30.5^m$ $\delta(\text{J2000}) = -16^\circ 40'$, which corresponds to Galactic coordinates $l = 249.2^\circ$, $b = +24.4^\circ$. We call this object G249+24. Below, we present images of this object’s UV and $H\alpha$ emission structure along with optical spectra of four of its filamentary regions.

3.2.1. Far UV Mosaic Image

Figure 7 presents a $5.2^\circ \times 5.2^\circ$ mosaic of GALEX FUV images centered on G249+24. The image shows several UV filaments along with a few smaller diffuse emission patches. Although GALEX imaging of this region is fairly incomplete, enough imaging exists to indicate G249+24’s minimum size and extent⁶.

The nebula’s brightest filaments are concentrated in its southern region where there is a bright, long gently curved filament along its southwestern edge. This feature itself consists of several separate, closely aligned filaments. Although a smaller but a similarly bright filament caught on the western edge of a more northern GALEX image might give the impression that this filament’s full length and extent is partially missing in this mosaic, this is not the case based on $H\alpha$ images (see below).

Along the northern portion of the FUV emission mosaic lies a fairly diffuse emission patch plus a few short faint filaments one of which is curved toward the bright SW filament. These features, taken together with the complex of southern filaments near $\delta = -19^\circ$, suggests the nebula has an angular N-S dimension around 4.2° . In contrast, its E-W dimensions are quite a bit less. A faint filament seen in G249+24’s southeastern region suggests an E-W dimension of $\approx 2.8^\circ$.

3.2.2. $H\alpha$ Emission

Whereas the object’s FUV emission filaments are readily apparent in the GALEX image mosaic shown

⁶ The bright feature at $9^h 30^m$, $-17^\circ 30'$ is HD 82093, an Ap(EuSrCr) star; $V = 7.08$.

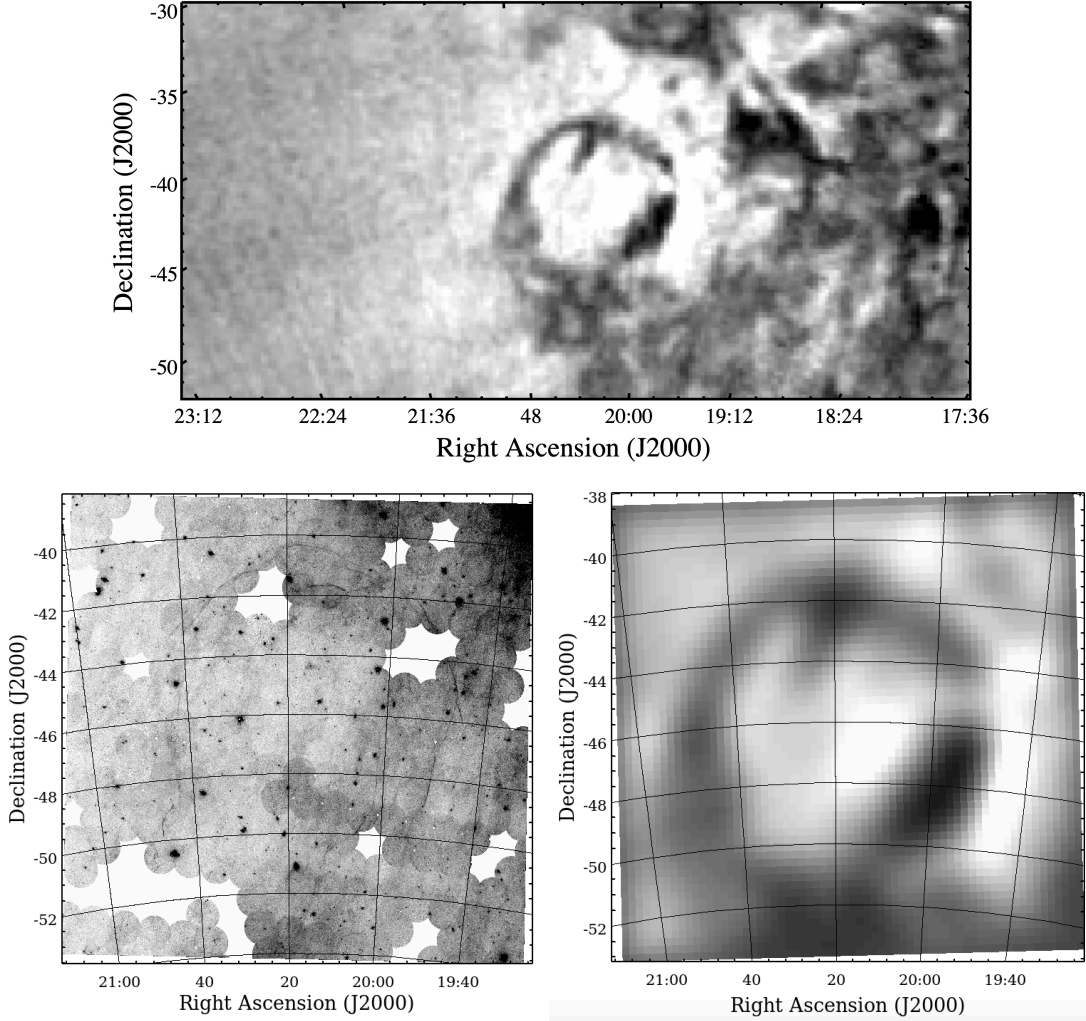


Figure 6. *Upper Panel* 1420 MHz Villa Elisa Stokes Q polarization intensity image covering a $60^\circ \times 25^\circ$ region centered on G354-33. *Lower Panels* : Comparison of the G354-33 region in the GALEX FUV image with the 1420 MHz image showing excellent size and positional agreement of the 1420 MHz radio emission ring with the shell of UV emission filaments.

in Figure 7, its optical emissions are relatively faint. Although some of its brighter filaments are weakly visible on broad red passband Digital Sky Survey images, they are so faint and scattered over such a large area that it is not surprising that this nebula had not attracted prior attention.

The $H\alpha$ images of the MDW All-Sky survey reveal more fully G249+24's optical emissions. In Figure 8, we show a side-by-side comparison of G249+24's central emission structure in GALEX FUV and the MDW $H\alpha$ images. In general, there is a good agreement between the nebula's UV and $H\alpha$ emissions. The bright FUV and curved southwestern filament shows up strongly in $H\alpha$ as does a shorter filament a degree to its east. Correlated UV – $H\alpha$ emission is also seen along the upper left-hand portion of Figure 8, where diffuse and filament type of emission is seen in both. (Note: Faint diffuse emission seen along the lower portion of the $H\alpha$ image extends

several degrees to both the east and west of the region and hence does not seem to be connected to G249+24's other optical features.)

However, little in the way of $H\alpha$ emission can be seen along the object's southeast limb, where in contrast one finds considerable FUV emission. A similar difference between FUV and $H\alpha$ fluxes is seen for the south-central area around $9^h 28^m, -18^\circ 15'$. Consequently, it is clear that this nebula's overall structure is more readily visible in the FUV than in even fairly deep $H\alpha$ images.

A few higher resolution $H\alpha$ images of selected regions of the nebula were also obtained. Although these images were taken in preparation of follow-up spectral observations, they showed considerably more detail to G249+24's filamentary emission than seen in Figure 8. Unfortunately given its large angular size, these comparatively small images serve only as a hint of the nebula's rich and detailed optical emission structure.

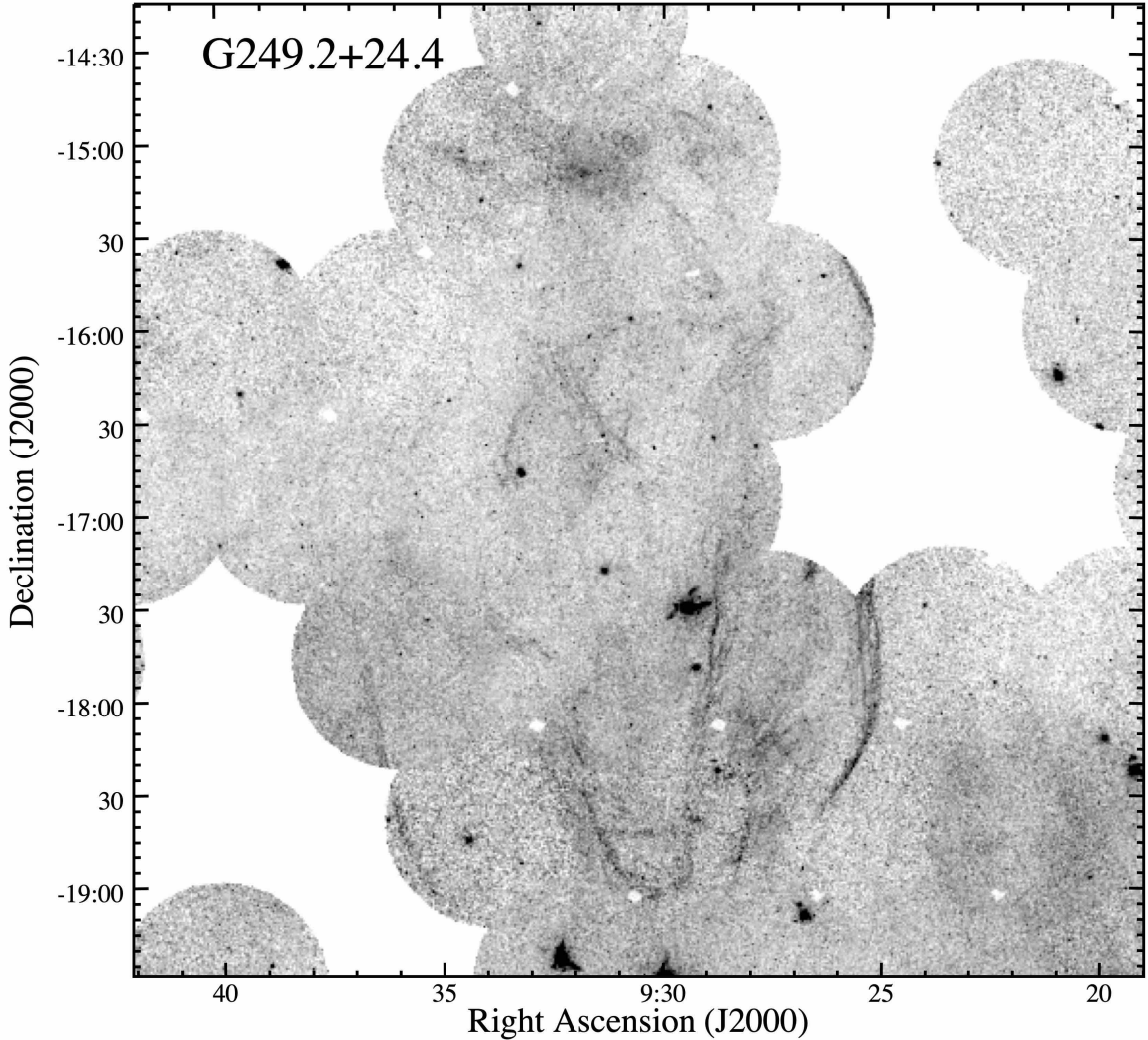


Figure 7. FUV intensity map of G249+24 showing an elliptical shaped shell of UV emission filaments.

3.2.3. Optical Spectra

Low-dispersion, exploratory slit spectra were taken at at four positions (P1 through P4) shown in Figure 9 to investigate the emission nature G249+24’s optical emission filaments. Figure 10 shows the resulting spectra covering the wavelength region 6200 to 6900 Å.

These spectra reveal evidence for its filaments as shock heated ISM like that commonly seen in SNRs. Spectra obtained at P2, P3 and P4 exhibited [S II]/H α ratios of 1.26 ± 0.20 , 0.45 ± 0.04 , and 0.91 ± 0.15 , respectively, thus well above the standard criteria ratio of 0.40 indicative of shock emission. Added support for shocks is the detection of [O I] $\lambda 6300$ emission in the spectra of both P3 and P4. The presence of [O I] is a secondary indicator for shock emission commonly observed in evolved SNRs (Fesen et al. 1985; Kopsacheili et al. 2020).

The [S II] $\lambda 6716/\lambda 6731$ line ratio can be used to estimate the electron density in the S⁺ recombination zone and is nearly independent of electron temperature (Os-

terbrock & Ferland 2006). The $\lambda 6716/\lambda 6731$ ratio was found to be near the low density limit of 1.43 indicating $n_e < 100 \text{ cm}^{-3}$; 1.48 ± 0.04 for P2, and 1.42 ± 0.03 for P4. A bit surprisingly, this ratio for P3 was observed to be $\simeq 1.15$ indicating an n_e density much higher than the other locations of around 500 cm^{-3} . Interestingly, the spectrum seen at P3 also showed much weaker [N II] $\lambda 6583$ line emission compared to that seen at P2 and P4.

The spectrum taken at P1 deserves special attention due to significant line emission variations with respect to distance along the E-W aligned slit. This is shown in Figure 11, where line emission can be seen to start at the location of the mainly N-S aligned filament extending many arcseconds to the east (left). The emission line ratio of H α /[O III] can be seen to vary considerably down stream from the shock front.

Figure 11 also shows the 2D image of the background subtracted P1 spectrum for the areas around H α , and [O III] $\lambda 4959$, $\lambda 5007$ and H β . This figure shows a clear

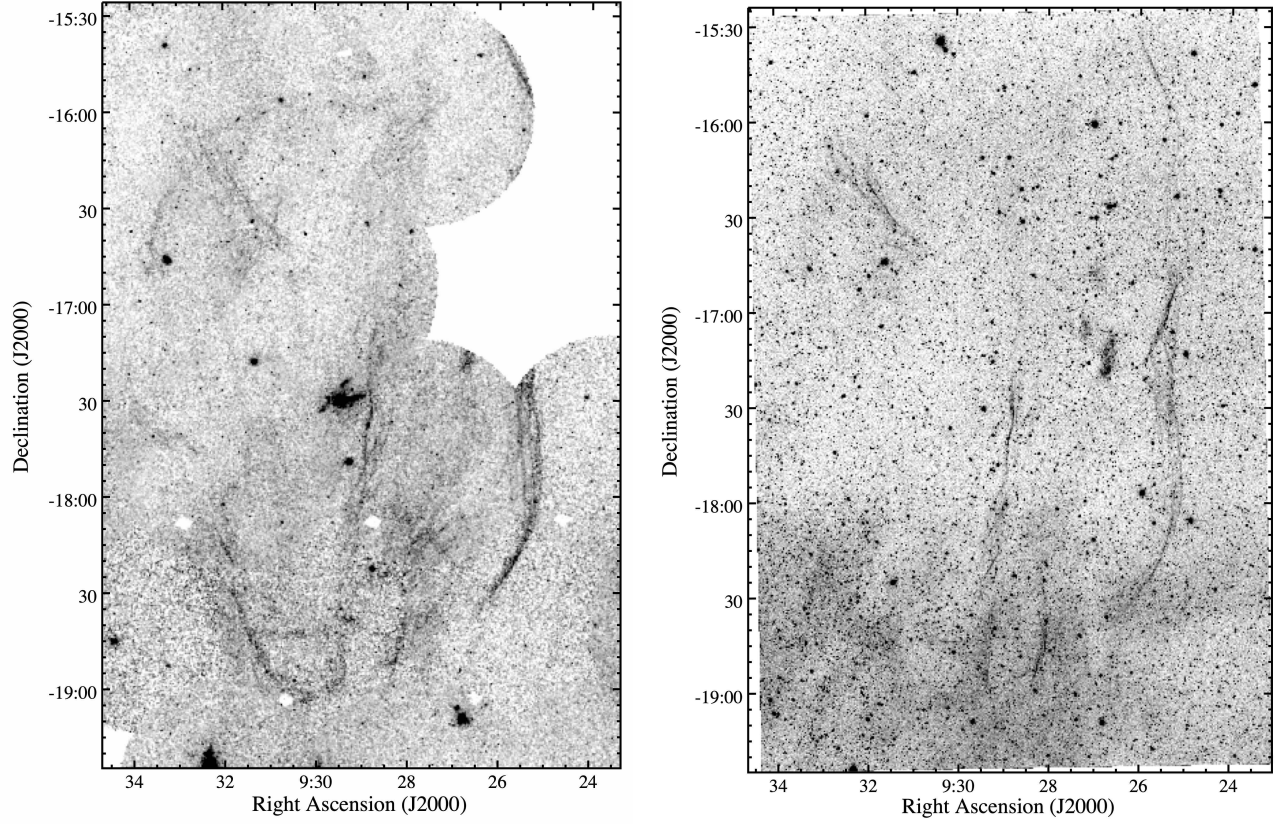


Figure 8. G249+24's FUV emissions (left) compared to its H α emission as seen in MDW's All-Sky H α Survey images (right).

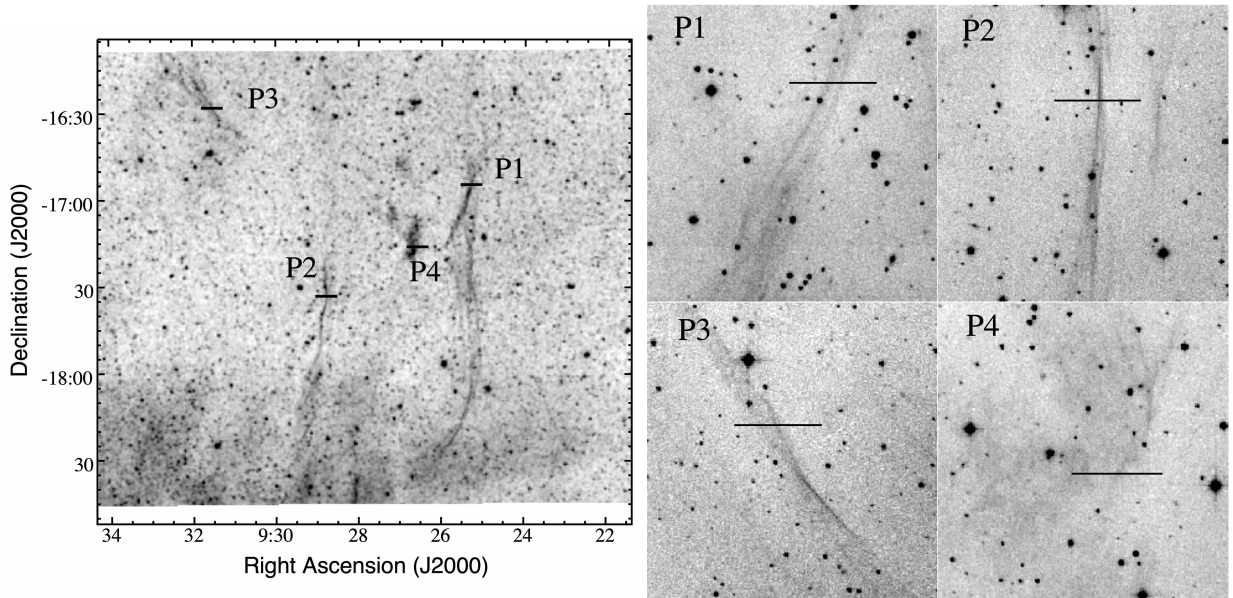


Figure 9. Left: MDW H α image of G249+24 showing the four locations where long slit spectra were taken. Right: Higher resolution of filaments and slit positions. Slit lengths as shown are $1.5'$.

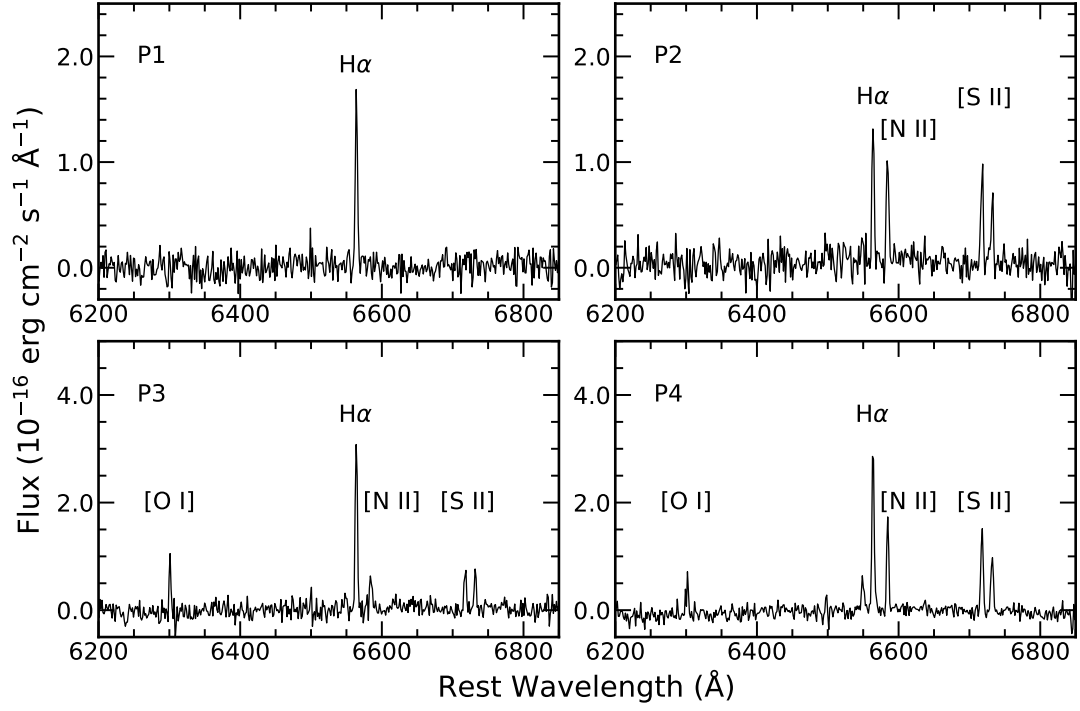


Figure 10. Spectra of four slit positions in G249+24.

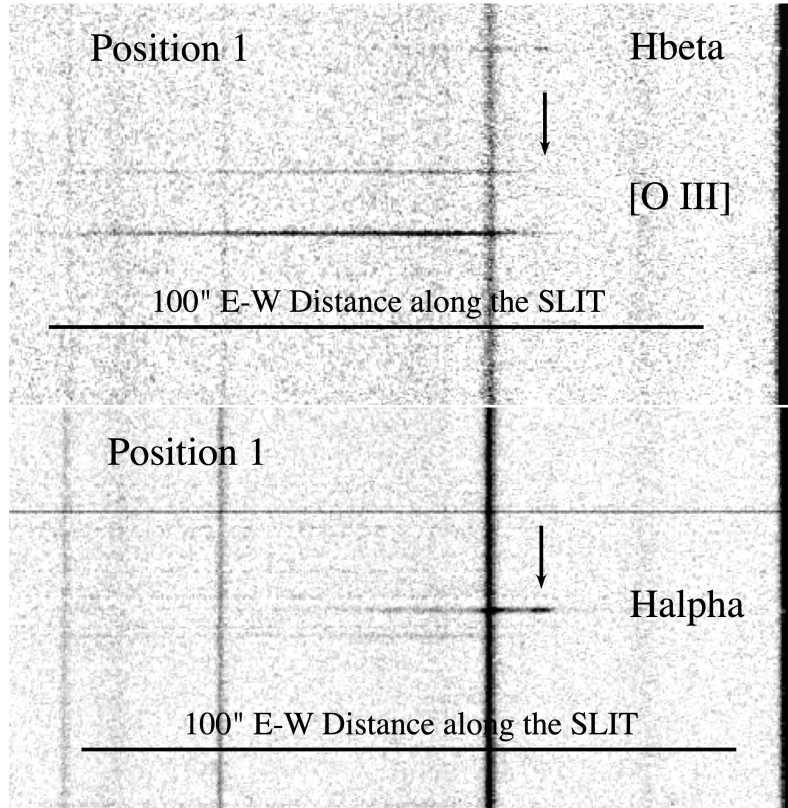


Figure 11. Sections of the long slit spectra for Position 1. Both [O III] $\lambda 4959$ and $\lambda 5007$ lines are visible in the upper panel.

separation of the filament’s Balmer dominated emission followed by strong [O III] emission resulting in large [O III] $\lambda 5007/\text{H}\alpha$ ratios. The arrows indicate the section where the P1 spectrum shown in Figure 10 was taken.

Behind the leading edge of the shock front marked by start of line emissions, $\text{H}\alpha$ emission becomes strong with little or no emission in other lines. The intensity of $\text{H}\alpha$ then briefly drops in strength within a distance of a few arcseconds, then increases for a short distance followed by a long, gradual decline. The [O III] emission is barely detectable at the shock front where the $\text{H}\alpha$ starts but substantially increases some 10-20 arcseconds behind the shock front to where it dominates the downstream spectrum. This is consistent with an extended post-shock cooling zone. The presence of such strong [O III] emission behind the shock front suggests shock velocities at least 100 km s^{-1} are present in certain filaments. In contrast, spectra at P2, P3, and P4 showed no appreciable [O III] emission.

Similar 2D emission structures were observed in the Galactic Halo SNRs G70.0-21.5 (Raymond et al. 2020) and G107.0+9.0 (Fesen et al. 2020). They can be interpreted as emission from a $\sim 100 \text{ km s}^{-1}$ shock in partially neutral gas. Neutral hydrogen atoms swept up by the shock are quickly ionized, but before that happens, some of them are excited to produce $\text{H}\alpha$. This emission region is very thin. It is followed by a thicker ionization zone where O II is ionized to O III. As the gas cools, the [O III] fades and $\text{H}\alpha$ brightens. In the case of G107.0+9.0, the $10''$ gap between $\text{H}\alpha$ and [O III] and the $\sim 10''$ wide diffuse patch of [O III] emission are well matched by models of 100 km s^{-1} shocks in a gas of density 0.1 cm^{-3} at a distance of 1 kpc (Fesen et al. 2020). The wider patch of [O III] diffuse emission at Position 1 of G249+24 suggests a longer cooling length, as would occur in a slightly faster shock, perhaps 120 km s^{-1} . These structures are spatially resolved thanks to the low density of the Galactic halo and the relatively small distances to these SNRs.

The flux level of $\text{H}\beta$ was either undetected or too faint at P2, P3, and P4 to accurately measure an $\text{H}\beta/\text{H}\alpha$ ratio which could be used to estimate extinction. Only the spectrum P1 showed a weak but measurable level of $\text{H}\beta$ flux. There the measured $\text{H}\alpha/\text{H}\beta$ ratio of 2.85 ± 0.20 suggests a very low amount of extinction. Adopting a theoretical $\text{H}\alpha/\text{H}\beta$ ratio of 2.87 for 10^4 K we estimate a foreground $E(B - V) < 0.07$. However, in view of the weakness of the $\text{H}\beta$ detection, this estimate comes with a large uncertainty. Nonetheless, such a low interstellar extinction is not unexpected due to the remnant’s high Galactic latitude of 24.4° .

If this low extinction estimate is correct, then the lack of [O III] emission at P2, P3, and P4 suggests a fairly low shock velocity, namely 70 km s^{-1} or less, in contrast to that indicated at P1. Consequently, it appears that a variety of shock speeds, from <70 to over 120 km s^{-1}

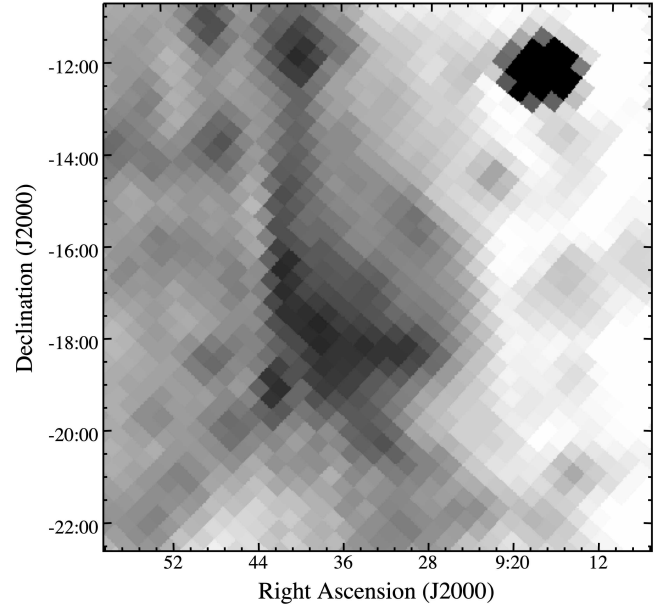


Figure 12. A 408 MHz intensity image of the G249+24 region from the Haslam et al. (1982) All-Sky survey.

appear to be present throughout the nebula’s structure, probably driven by an inhomogeneous local ISM.

3.2.4. Associated Radio and X-Ray Emissions

Examination of several on-line radio maps including the NRAO VLA Sky Survey (NVSS; Condon et al. 1998) did not show obvious radio emission in the G249+24’s region. However, the 1420 MHz Bonn survey (Reich 1982) did show some emission along G249+24’s FUV and optical filaments near $\alpha(\text{J2000}) = 9^{\text{h}} 27.5^{\text{m}}$, $\delta(\text{J2000}) = -16^\circ 10'$.

The 408 MHz all-sky survey (Haslam et al. 1981, 1982) also showed enhanced emission in a roughly spherical shape approximately 4° in diameter and centered at $9^{\text{h}} 32.7^{\text{m}}$, $-16^\circ 45'$, a position that is nearly the same indicated by FUV and optical images (see Fig. 12). A seemingly unrelated broad, vertical emission feature borders the emission shell on its eastern side and complicates the assessment of this emission. If this emission shell is associated with the nebula, it would suggest a far more spherical SNR than indicated by either the FUV or $\text{H}\alpha$ images.

Regarding possible X-ray emission, we note that the recently published low-resolution SRG/eRosita all-sky X-ray image⁷ (Predehl et al. 2020) shows a faint shell of soft X-ray emission at an usually high Galactic latitude in a location consistent with it possibly being associated

⁷ Sanders, J. et al. Annotated version of the eROSITA first all-sky image. [http://www.mpe.mpg.de/7461950/erass1-presskit\(2020\)](http://www.mpe.mpg.de/7461950/erass1-presskit(2020))

with this apparent SNR. Investigation of this interesting and extended X-ray feature is strongly encouraged.

3.3. *The Exceptionally Large Suspected Antlia SNR*

McCullough et al. (2002) reported a discovery of a very large 24° diameter $H\alpha$ emission shell with interior ROSAT 0.25 keV X-ray emission located in the southern hemisphere and at a high Galactic latitude of $+19^\circ$. They proposed it to be a previously unrecognized SNR and named it Antlia for the constellation it lies in. McCullough et al. (2002) suggested it was an extremely old remnant with an estimated age of ~ 1 Myr and located relatively nearby with an uncertain distance of between 60 pc and 340 pc.

The Antlia remnant does appear in the catalogue of high energy SNRs (Ferrand & Safi-Harb 2012) but not in the Green (2019) catalogue of confirmed Galactic SNRs, which cited the need for further observations to confirm its nature and parameters. Except for a 2007 far UV study finding weak coincident C III $\lambda 977$ and C IV $\lambda\lambda 1548, 1551$ line emissions from the object's interior (Shinn et al. 2007), there does not appear to have been much follow-up investigation of this exceptionally large suspected SNR. This situation plus its location at an unusually high Galactic latitude led us to include it in our high Galactic latitude GALEX FUV investigation of SNRs.

3.3.1. *GALEX FUV and MDW $H\alpha$ Images*

In the top panel of Figure 13, we present a mosaic of SHASSA $H\alpha$ images of the Antlia remnant at a higher resolution than the VTTS $H\alpha$ image (Finkbeiner 2003) which led McCullough et al. (2002) to discover it. It shows a $\sim 20^\circ \times 26^\circ$ $H\alpha$ emission shell with a well determined boundary roughly centered at $\alpha(J2000) = 10^h 38^m$, $\delta(J2000) = -37^\circ 18'$ corresponding to Galactic coordinates $l = 275.5^\circ$ $b = +18.4^\circ$. (Note: These Galactic coordinates differ slightly from those given by McCullough et al. 2002.)

A mosaic of FUV GALEX images covering just the remnant's northern limb is shown in the lower panel of Figure 13. This image reveals a long and nearly continuous set of thin, bright FUV emission filaments and filament clusters extending approximately 20 degrees along the remnant's northeastern limb. The line of FUV filaments starts at RA = $10^h 10^m$ and Dec = -24° and extends southward to the bottom left of the figure at RA = $11^h 40^m$ and Dec = -32° .

Because the morphology of Antlia's FUV filaments is similar to that seen in the proposed SNRs G354-33 and G249+24, we examined MDW $H\alpha$ images of the FUV filaments and adjacent regions above the -32° Declination limit of the MDW survey. Overall, we found excellent positional agreement between FUV and $H\alpha$ filaments.

To illustrate this agreement Figure 14 shows a comparison of GALEX FUV and MDW survey $H\alpha$ images for three sections along the Antlia's northeastern bound-

ary. While we find there is a close correlation of the outer FUV filaments with many $H\alpha$ filaments, there are also considerable differences in terms of the nebula's internal emissions. That is, far more $H\alpha$ emission is seen 'behind', i.e., to the west, of the sharp, outlying filaments than seen in the FUV images. This is most striking in the lower panel images of Figure 13 for the remnant's southeastern limb region. While the SHASSA image shows considerable internal diffuse and filamentary emission, the brightest $H\alpha$ emissions are found along Antlia's northwestern, western and southeast limbs.

3.3.2. *Optical Spectra*

If McCullough et al. (2002) is correct in their assessment that the Antlia $H\alpha$ nebula is a SNR, as seemingly supported by the GALEX FUV and $H\alpha$ images described above, the remnant would then be both many times larger than any confirmed SNR and be located at an unusually high Galactic latitude. On the other hand, considering its location immediately adjacent to the enormous Gum Nebula with its extended emission, outer 'filamentary wisps', and numerous H I wind blown bubbles (Brandt et al. 1976; Chanut & Sivan 1983; Purcell et al. 2015), there is real uncertainty about its true origin.

Optical spectra are a powerful tool for confirming the presence of shock emission and hence can be used to investigate the SNR origin of optical nebulosities. Consequently, we obtained long-slit, low-dispersion spectra of seven filaments and emission clumps distributed across the whole of the Antlia nebula to explore the nature of its optical emissions.

Figure 15 shows the location of the seven filaments observed in the Antlia remnant, along with the resulting spectra. Table 2 lists the relative emission line strengths uncorrected for extinction. Listed relative line strengths are believed accurate to 10%. Based on the observed $H\alpha/H\beta$ ratios of 3.0 to 4.30, we find a variable degree of extinction across the Antlia nebula, with $E(B - V)$ values ranging from 0.0 to 0.35 assuming an intrinsic ratio of 3.0 and an R value of 3.1. Here we have chosen an $H\alpha/H\beta$ value greater than the theoretical value of 2.87 for 10^4 K due to the likelihood of significant collisional excitation of the $n = 3$ level at postshock temperatures seen in SNRs. Such a range of extinction values is not unexpected in view of the nebula's large dimensions.

These optical spectra show clear evidence that the seven filaments observed distributed across the whole of the Antlia nebula exhibit line ratios indicative of shock emissions. In fact, emissions at Positions 4 and 6, located along Antlia's southeastern limb display non-radiative, pure Balmer line emission.⁸ Such shock spectra are usually seen in situations where the shock ve-

⁸ Note: The [O I] emission seen in the spectrum for Position 4 is residual imperfect [O I] sky emission.

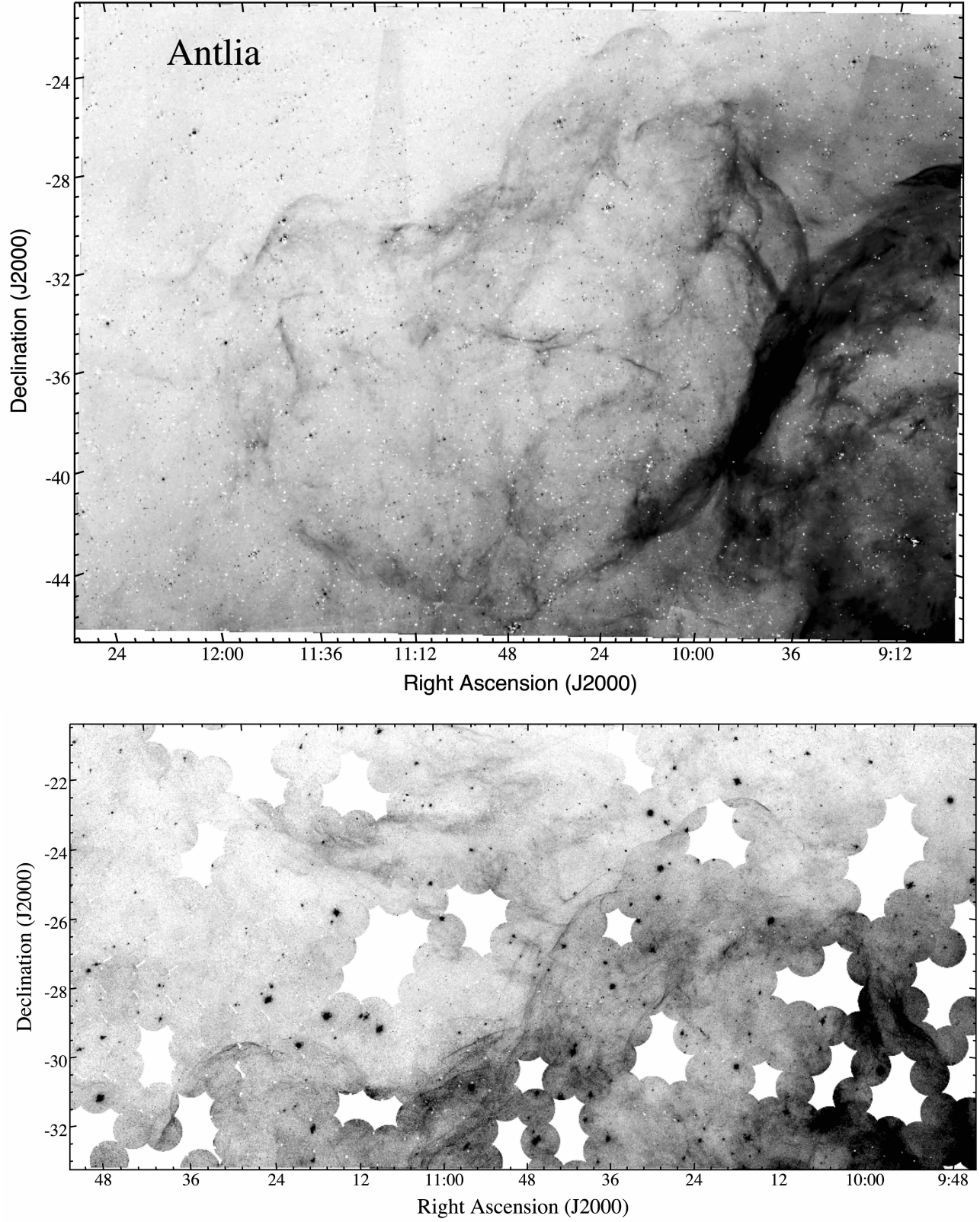


Figure 13. *Top* : Continuum subtracted SHASSA $H\alpha$ image mosaic of the Antlia remnant. *Bottom* : GALEX FUV mosaic showing a nearly unbroken line of UV emission filaments along Antlia's northern and eastern boundary.

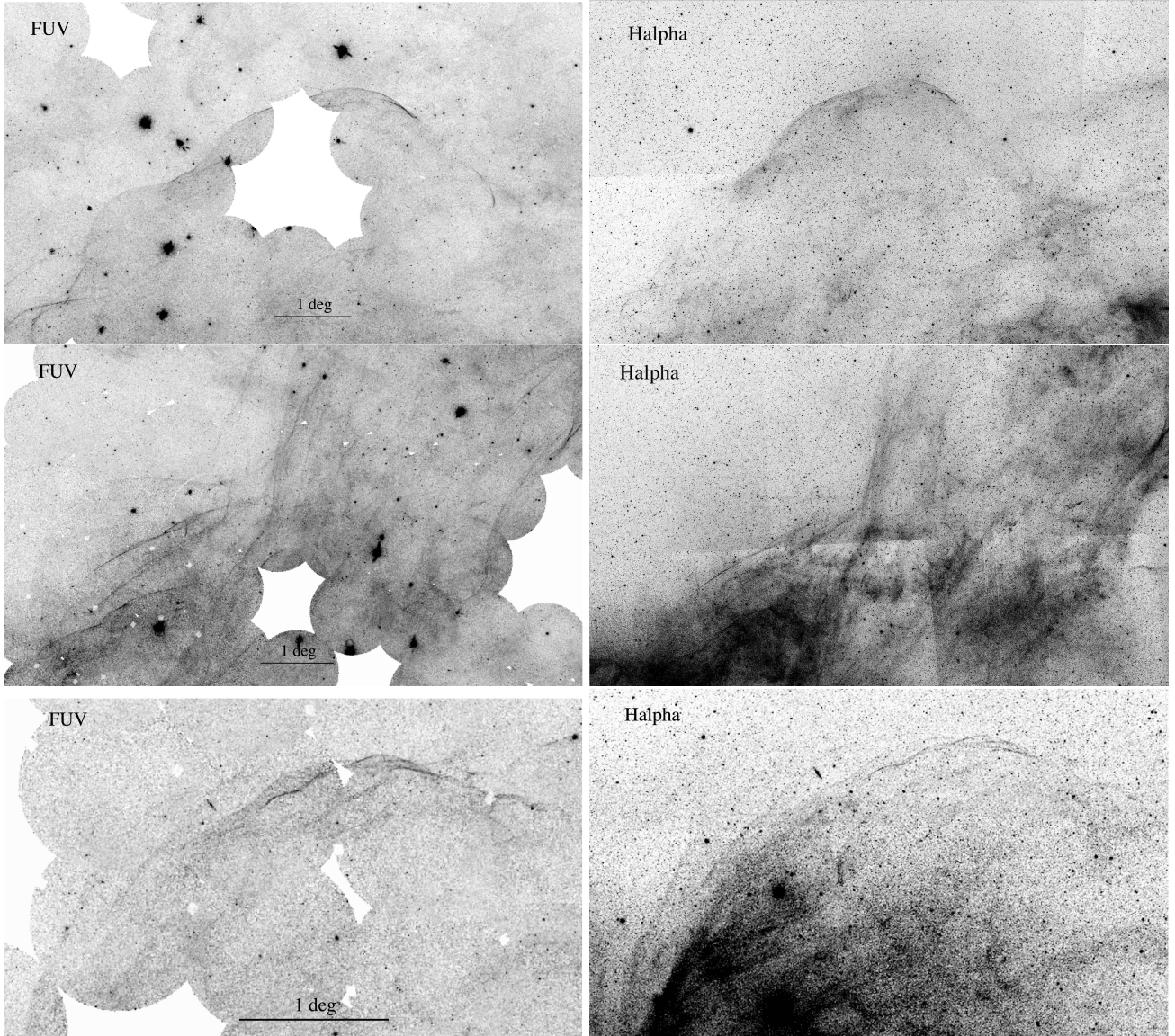


Figure 14. Comparison of GALEX FUV emission vs. MDW $H\alpha$ image mosaic of the northern, eastern, and southeastern portions of the Antlia SNR showing a close agreement of UV and $H\alpha$ emission filaments along its eastern boundary. There is considerable $H\alpha$ emission but little FUV emission in the nebula's interior.

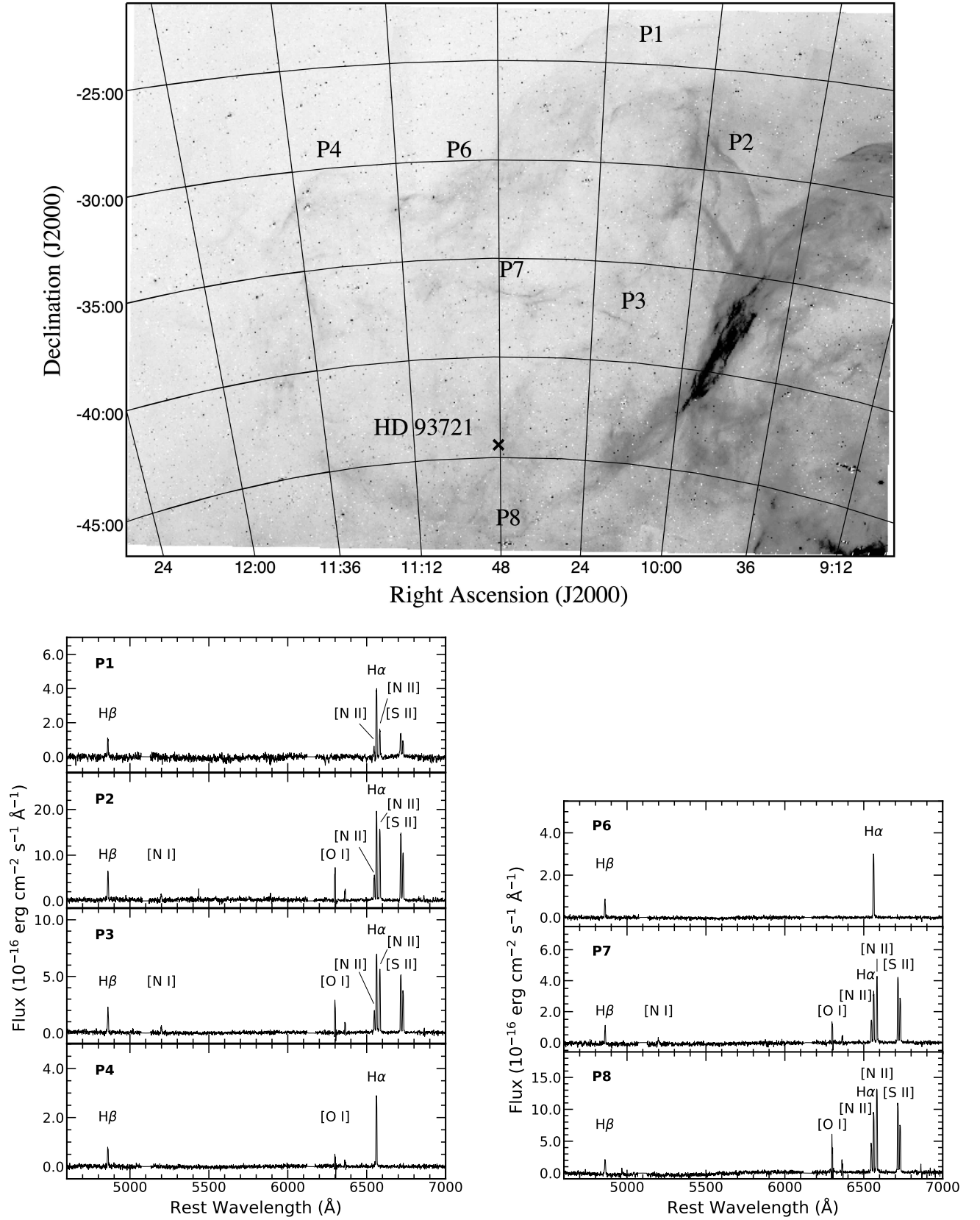


Figure 15. Top: Continuum subtracted SHASSA H α image mosaic of the Antlia remnant showing the locations of seven positions where SALT spectra were obtained. Bottom panels: Observed optical spectra at these seven positions.

locities are quite high ($> 500 \text{ km s}^{-1}$) as seen in young Type Ia SNRs like Tycho and SN 1006. However, similar Balmer dominated spectra has also been seen in much older remnants (G107.+9.0; Fesen et al. 2020). Relatively slow shocks can remain non-radiative if the ambient density is sufficiently low, like that expected in the Galactic halo. This requires that the cooling time of the shocked gas should be long enough to prevent the forbidden lines from becoming bright. Scaling the cooling times of Hartigan et al. (1987) with n_0^{-1} , the non-radiative shocks at the edge of a 100,000 year old remnant in a density of 0.1 cm^{-3} would be at least 170 km s^{-1} .

The other five filaments show optical spectra commonly seen in evolved SNRs like the Cygnus Loop and IC 443. In all these cases, the [S II] $\lambda 6716/\lambda 6731$ ratio exceeds the 0.4 criterion for shock emission. Indeed, filaments 7 and 8 display ratios above 2, which are among the highest values observed in SNRs. Interestingly, these five filaments lack appreciable [O III] $\lambda\lambda 4959, 5007$ emission. Weak or absent [O III] emission indicates shock velocities less than about 90 km s^{-1} . The high $\text{H}\alpha/\text{H}\beta$ ratio in Position 1 of the Antlia remnant suggests a substantial contribution of collisional excitation at fairly low temperatures to the Balmer lines, and this is borne out by the low [N II] and [S II] to $\text{H}\alpha$ ratios. That suggests shock speeds around 70 km s^{-1} . Given these slow shock spectra along with pure Balmer emission spectra along the remnant's leading edges, there must be a considerable range of shock velocities present in the nebula. This is not too surprising given the large size of Antlia and a nearly 18° range in Galactic latitude.

4. DISCUSSION

Based on the data presented above, we find that two high latitude suspected SNRs, namely G354-33 and Antlia, are likely bona fide SNRs. Moreover, their UV emission filaments appear best at marking these objects' forward shock front locations. Below we discuss supporting evidence for our conclusions, followed by estimates regarding their true physical dimensions and general properties. We then briefly comment of the usefulness of far UV imaging for SNR detection particularly in areas far off the Galactic plane.

4.1. G353.9-33.4

There are several observations that support the SNR identification of this large FUV, $\text{H}\alpha$, and radio nebula. At its Galactic latitude of -33.4° , there are no bright and nearby early type stars near the center of this UV shell that might have generated its UV emission shell through stellar winds. There is also no known nearby recurrent nova projected inside, and the emission shell is at least two orders of magnitude larger and does not have a similar appearance to known nova shells.

Then there is the large 1420 MHz radio emission shell roughly centered on and lying entirely within the bor-

ders of the FUV emission filaments. The FUV filaments also exhibit a shock-like morphology such as commonly seen in Galactic SNRs. Furthermore, its nearly continuous ring of thin filaments surrounds a broad, diffuse $\text{H}\alpha$ emission shell. So in summary, its shock-like filamentary appearance and the positional agreement between UV, $\text{H}\alpha$ and radio emissions for such a large object located far off the Galactic plane leaves few viable options other than a SNR origin.

While we have not yet been able to obtain optical spectra of its $\text{H}\alpha$ and UV filaments to test this conclusion, we suspect this remnant may resemble that of the high-latitude remnant, G65.3+5.7 (Gull et al. 1977; Boumis et al. 2004). That remnant also exhibits strong far UV emissions (Kim et al. 2010) with few $\text{H}\alpha$ bright filaments across the whole of its $3^\circ \times 4^\circ$ shell. Because most of the G65.3+5.7 filaments are brightest in [O III] line emission, if G354-33 is similar, then its spectrum might also show strong [O III] line emissions and hence be most apparent in wide-angle [O III] imaging.

Centered at a Galactic latitude around -33.4° , G354-33 ranks as the highest Galactic latitude SNR found yet. In addition, if not for the Antlia remnant, this object would also rank first in angular dimensions among the roughly 300 SNRs in the Green (2019) catalogue. Because of its $\sim 11^\circ \times 14^\circ$ size and the fact that the largest known SNRs have physical dimensions $\sim 100 \text{ pc}$, we can make some crude estimates of its distance and properties.

As shown in Table 1, if its diameter is taken to be 100 pc , then its distance is around 400 pc . Based on the presence of its stronger FUV than NUV emission, its shock velocity is likely greater than 100 km s^{-1} but probably less than 150 km s^{-1} , according to Figure 4 of Bracco et al. (2020). That shock speed is too high for this remnant to be in the snowplow phase of SNR evolution, but the presence of radiative shock waves around much of the rim indicates that it is no longer in the Sedov phase, at least in those places. That suggests that it is in the pressure-driven shell phase, when the recently shocked gas has cooled, but there is still relatively hot, high-pressure gas in the interior.

From the calculations of Cioffi et al. (1988), this velocity range and a diameter of around 90 pc would be consistent with an age $\simeq 10^5$ years and a preshock density of 0.1 cm^{-3} (see Fig. 14 of Fesen et al. 2020). One might expect detectable X-ray emission during the pressure-driven shell phase, but Shelton (1998) has discussed halo SNRs in which the interior gas is too cool to produce X-rays, but still rich in high ionization states such as O VI.

4.2. G249.2+24.4

The evidence for identifying this nebula as a SNR is compelling. Both GALEX FUV and SHASSA $\text{H}\alpha$ images display a highly filamentary morphology like that seen in SNRs, and optical spectra that show emission line ratios consistent with the presence of shocks. The

Table 2. Observed Emission Line Fluxes for Antlia Filaments

Emission Line (Å)	Filament Position						
	P1	P2	P3	P4	P6	P7	P8
H β 4861	100	100	100	100	100	100	100
[O III] 5007	< 10	< 10	< 10	< 10	< 10	< 10	< 10
[N I] 5200	...	23	29	20	...
[O I] 6300	...	93	98	101	122
[N II] 6548	57	89	97	137	181
H α 6563	430	300	339	379	368	304	365
[N II] 6583	167	247	275	403	542
[S II] 6716	146	239	247	406	442
[S II] 6731	91	167	184	283	307
F([S II])/F(H α)	0.55	1.35	1.27	2.27	2.05
[S II] 6716/6731	1.60	1.43	1.34	1.43	1.44
$E(B - V)$	0.35	0.00	0.12	0.23	0.20	0.01	0.19
F(H α) erg cm ⁻² s ⁻¹	2.74E-15	1.29E-14	4.75E-15	1.91E-15	2.06E-15	2.16E-15	6.06E-15

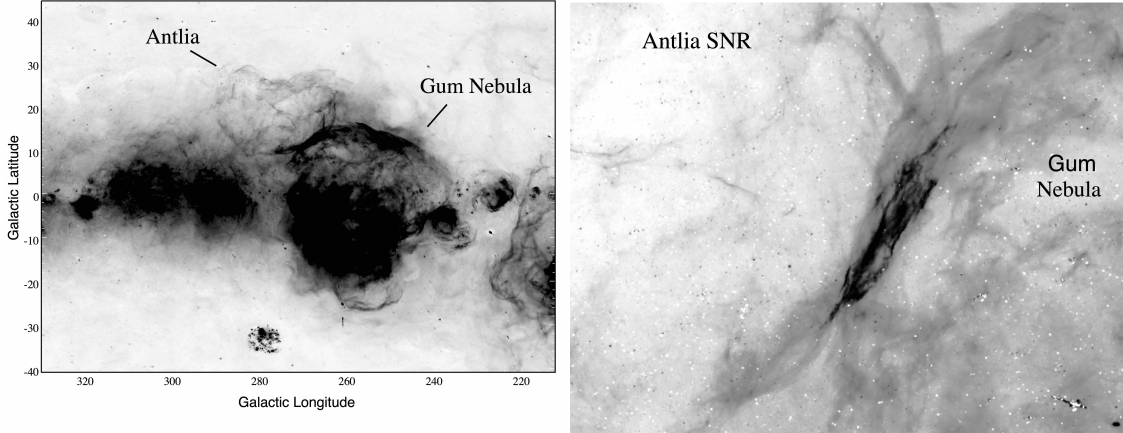


Figure 16. *Left* : VTTs H α image of the Galactic plane around the Gum Nebula with the location of the Antlia SNR marked. *Right* : The continuum subtracted SHASSA H α image of the Antlia remnant showing the presence of bright filaments at the overlapping Antlia and Gum Nebula region suggestive of physical interaction.

added presence of coincident radio and possibly X-ray emissions leaves little doubt that this object is likely a true SNR.

With a size of $2.8^\circ \times 4.2^\circ$, this object exhibits angular dimensions among the largest of previously known SNRs. In addition, it being situated at Galactic latitude of over 24 degrees, G249+24 lies farther from the Milky Way's plane than any other confirmed SNR – that is, other than G354-33.

Although we do not know its distance, we can make estimates of its shock velocities based on our optical spectra which, in turn, can be used to constrain both its distance and age. Based on its optical emissions, along

with the strength of [O III] emission and the presence of Balmer dominated emission detected at slit P1, shock velocities of at least $70 - 100 \text{ km s}^{-1}$ appear present in the remnant. Following the discussion above for G354-33, we estimate a radius $\sim 30 - 40 \text{ pc}$ assuming $E_o = 1 \times 10^{51} \text{ erg}$, $n_o = 1 \text{ cm}^{-3}$, and a blast velocity of $100 - 150 \text{ km s}^{-1}$. Adopting a radius of 35 pc means G249+24's angular diameter of 4.2 degrees suggests a distance around 1 kpc. As with G354-33, this SNR is likely to be in the pressure-driven shell phase. Its physical size is probably smaller and the shock speed larger, so Figure 14 of Fesen et al. (2020) suggests an age closer to $80 \times 10^3 \text{ years}$.

4.3. The Nature of the Antlia Nebula

McCullough et al. (2002) claimed this extraordinarily large emission nebula was a likely SNR based on its appearance on the deep H α image of the VTTS survey and on the presence of diffuse soft X-ray emission in its interior. However, this conclusion does not appear to be widely accepted, as measured by the remnant having attracted little subsequent attention.

This situation might in part be due to a reluctance by SNR researchers to accept its huge $20^\circ \times 26^\circ$ size, more than 3-5 times larger than the largest known confirmed SNRs, plus its location so close to the even larger Gum Nebula with its complex of large emission shells and wind-blown bubbles and the huge Vela SNR. Consequently, except for a far UV study by Shinn et al. (2007), the Antlia remnant has not yet been studied in any detail, leaving open its true nature.

Our GALEX FUV mosaics show a well-defined shell in H α with many individual and overlapping filaments that closely resemble shocks. In addition, the locations of these sharp UV filaments along the boundary of the object's H α emission are consistent with a SNR where such UV filaments mark the location of the remnant's shock front.

Importantly, results of our seven optical spectra of Antlia's filaments argue for shock emissions throughout the nebula thereby leading to it being a SNR. These spectra include two textbook cases of non-radiative Balmer dominated spectra (Positions 4 & 6), plus several other filaments exhibiting high [S II]/H α line ratios well above the 0.4 value distinguishing shocked from photoionized nebulae. If the Antlia remnant was not so large, it would be a easy case for supernova remnant classification.

Unfortunately, the physical size of the Antlia SNR is unknown due to its unknown distance. McCullough et al. (2002) estimated a wide range of possible distances, from 60 pc to 320 pc, and believed the remnant to be extremely old, at least 1 Myr, and hence in the final snowplow phase of SNR evolution. However, our optical spectra do not support such an old object or a distance less than 200 pc. A 1 Myr old SNR is expected to have a very low expansion velocity of around 10 to 20 km s $^{-1}$ (Chevalier 1977).

However, our optical spectra show line emissions indicating shock velocities of 50 to 150 km s $^{-1}$, making it far younger ($< 10^5$ yr) and in the pressure-driven shell phase. Moreover, there are additional data supporting high-velocity gas inside a much younger Antlia remnant.

Before the Antlia nebula was discovered, Bajaja et al. (1989) found high-velocity clouds in the remnant's direction, and Penprase & Blades (1992) reported detecting high-velocity Ca II absorption lines in the spectrum of the B9/A0 III/IV star HD 93721 which lies in the direction of the Antlia SNR (see Fig. 15). This star has a estimated Gaia Early Data release distance of 512 ± 7

pc. Penprase & Blades (1992) found at least 10 Ca II absorption components with v_{lsr} ranging from -65 km s $^{-1}$ to $+75$ km s $^{-1}$. Because a second star, HD 94724 ($d = 210$ pc) lying in the same general direction did not show any high-velocity components, they concluded that the high-velocity absorbing cloud's distance was between 200 and 500 pc. However, because not all stars behind a SNR display high-velocity absorption lines, a lack of high-velocity components does not provide a robust minimum distance estimate.

An alternative means of estimating the distance to the Antlia remnant is its apparent collision with the 36° diameter Gum Nebula (Gum 1952, 1955; Brandt et al. 1971; Sivan 1974; Chanot & Sivan 1983). Although the coincidence of the remnant's southwestern rim with the Gum Nebula's bright northeastern emission cloud has been noted in a few studies of the Gum Nebula (Iacobelli et al. 2014; Purcell et al. 2015), no mention has been made about a physical interaction between the two.

However, our SHASSA imaging mosaic strongly indicates such collision has occurred between the Antlia remnant and the Gum Nebula. To begin with, the left panel of Figure 16 presents a section of the VTTS H α image of the Galactic plane showing the Antlia emission shell, similar to the VTTS image presented in the McCullough et al. (2002) Antlia discovery paper. This shows Antlia's position relative to the Gum Nebula. The remnant's bright southern limb coincides with the northern rim of the Gum Nebula.

The right panel of Figure 16 shows a low contrast version of our SHASSA image of Antlia. A line of long, bright filaments can be seen in the projected overlap region of both shells (see also Fig. 15). The simplest explanation for such bright filaments situated only in the exact Antlia/Gum overlap region is that the Antlia remnant has collided with the outer northeastern rim of the Gum Nebula.

If that is correct, then the Antlia's distance is roughly the same as for the Gum Nebula. Unfortunately, the distance to the Gum Nebula is poorly known, with values ranging from 200 – 500 pc (Brandt et al. 1971; Woermann et al. 2001; Howarth & van Leeuwen 2019). However, at the least, distances below 200 pc like suggested by McCullough et al. (2002) would appear to be ruled out. If we adopt a distance of 300 pc, like that estimated for some of the Gum Nebula's ionizing stars (Howarth & van Leeuwen 2019), then, the Antlia remnant's physical diameter is ~ 120 pc.

4.4. The Power of FUV Emissions for Finding SNRs

A few large Galactic SNRs and superbubbles have been recently studied in terms of their far UV emissions. For example, studies of far UV emissions have been reported for the Vela SNR (Nishikida et al. 2006), the Cygnus Loop (Seon et al. 2006), the Lupus Loop (Shinn et al. 2006), and the Orion-Eridanus Superbubble (Kregenow et al. 2006). Many of these made use

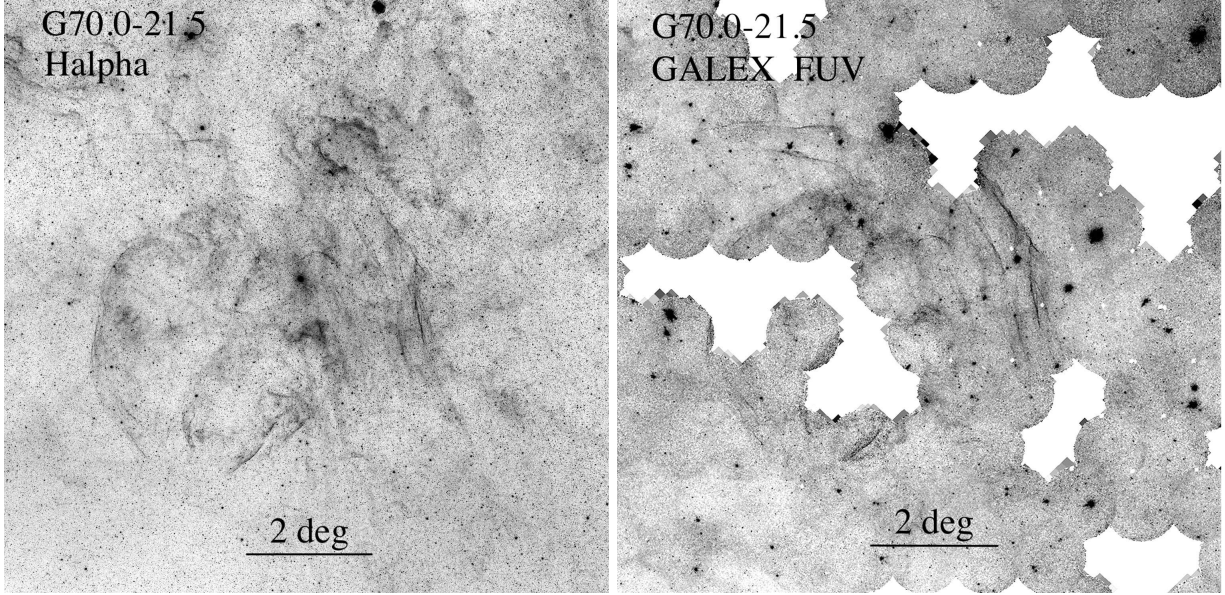


Figure 17. Comparison of MDW $H\alpha$ and GALEX FUV images of the high-latitude remnant G70.0-21.5. North is up, East to the left.

of the SPEAR imaging spectrograph (Edelstein et al. 2006).

However, there have been few papers reporting discoveries of large interstellar emission structures using FUV emissions. One such paper is that of Bracco et al. (2020) who reported finding a 30° long UV arc in Ursa Major using GALEX images. That work was a follow-up to an earlier detection of a much shorter 2.5° filament by McCullough & Benjamin (2001) using deep $H\alpha$ imaging. However, only through the GALEX’s FUV images was the full extent of this faint, long interstellar filament finally revealed.

The FUV emission of moderate velocity shocks is dominated by the hydrogen 2-photon continuum, resonance lines of C IV and Mg II, and intercombination lines such as C III] and Si III]. Bracco et al. (2020) computed the GALEX FUV and NUV count rates for shocks from the Sutherland & Dopita (2017) MAPPINGS models. Shocks slower than about 100 km s^{-1} are dominated by the 2-photon continuum, while faster shocks have strong contributions from C IV and other lines. The predicted ratios range from about 0.1 to 0.9. Based on our own model calculations, a reddening $E(B - V) \sim 0.1$ does not affect the ratios very much, though it reduces both the NUV and FUV count rates by a factor of 2. A major caveat, however, is that scattering in edge-on sheets of emitting gas, in particular SNR filaments, can strongly reduce the intensities of resonance lines such as C IV (Cornett et al. 1992), reducing the FUV/NUV ratio.

Above we have presented large GALEX FUV mosaic images of two large nebulae which appear to be true Galactic SNRs, but were either only suspected or missed in most radio studies which have concentrated their searches near the Galactic plane. The object G249+24

appears to have been missed in wide FOV optical surveys due to its relatively weak $H\alpha$ emissions.

Both our investigations and that of Bracco et al. (2020) indicate that broad, far UV imaging can be an especially useful means for detecting and distinguishing interstellar shocks and, in some cases, is more sensitive compared to $H\alpha$ imaging. As noted by Bracco et al. (2020), both line emissions and two photon continuum emissions contribute to FUV emission in shocks with velocities above $\simeq 50 \text{ km s}^{-1}$.

To illustrate the usefulness of far UV emission imaging for detecting SNRs, Bracco et al. (2020) noted the presence of networks of thin FUV filaments in both the Antlia SNR and the recently discovered Galactic remnant G70.0-21.5 (Boumis et al. 2002; Fesen et al. 2015; Raymond et al. 2020). In Figure 17 we show a comparison of MDW’s $H\alpha$ image and the GALEX FUV image of G70.0-21.5. Until the study of the SNRs discussed here, this remnant at $b = -21.5^\circ$ had been the remnant with the highest Galactic latitude. This figure amply demonstrates how that the FUV image makes the remnant much easier to detect and helps to define its full dimensions despite the many missing individual GALEX images. Knowing about the existence of these GALEX FUV images could have helped Fesen et al. (2015) and Raymond et al. (2020) in their analysis of this remnant in regard to the remnant’s true physical size. In summary therefore, far UV images appear to be an especially useful tool for identifying interstellar shocks like those found in SNRs, albeit though best suited for high Galactic latitude searches.

5. CONCLUSIONS

We have investigated the nature of two large and suspected supernova remnants located at unusually high Galactic latitudes through GALEX far UV emission mosaics and optical images and spectra. This research also has uncovered one new Galactic SNR. Our findings include:

1) The large $\sim 10^\circ$ radio emission shell, G353.9-33.4, seen in 1420 MHz and 1.4 GHz radio polarization maps is very likely a SNR. The remnant exhibits numerous sharp FUV emission filaments in a thin, unbroken shell with angular dimensions of $11^\circ \times 14.0^\circ$. It also exhibits a coincident $H\alpha$ emission shell.

2) A group of bright, sharp FUV emission filaments extending some $2.8^\circ \times 4.2^\circ$ in size and coincident with numerous but faint $H\alpha$ filaments appears to be a previously unrecognized SNR. Optical spectra of several filaments show evidence for the presence of 50 - 150 km s $^{-1}$ shocks. Deep $H\alpha$ images reveal a highly filamentary morphology like that seen in evolved SNRs. Coincident diffuse 408 MHz radio emission lends additional support for its SNR identification.

3) Despite its enormous angular dimensions ($20^\circ \times 26^\circ$), GALEX FUV mosaic images, plus wide-angle $H\alpha$ images and optical spectra strongly support a SNR origin for the Antlia nebula. This conclusion is in line with ± 70 km s $^{-1}$ Ca II absorptions in one background star. We estimate an age $\sim 10^5$ yr, which is an order of magnitude less than the earlier estimate of 1 Myr. We also find the remnant is in likely physical contact along its southwestern rim with the Gum Nebula which could help constraint its distance.

4) Our investigation of suspected SNR located at unusually high Galactic latitudes ($> 15^\circ$) highlights the value of UV images to detect interstellar shocks.

Follow-up work on these three objects could include optical spectra of the FUV and $H\alpha$ filaments of the G354-33 remnant, and wide-field [O III] $\lambda 5007$ imaging of G354-33 and G249+24 since both might exhibit especially bright [O III] filaments. Higher resolution $H\alpha$ images and optical spectra of the series of long and very bright filaments seen in southwestern limb of the Antlia remnant could also provide a test of our conclusion regarding Antlia's collision with the Gum Nebula.

Although we have found that all three nebula in our study are SNRs, none have accurate distance estimates, leaving us with only approximate physical parameters

and evolutionary status. This problem can be addressed especially well in the era of accurate Gaia parallaxes through high-dispersion spectra looking for high-velocity Na I $\lambda\lambda 5890, 5896$ and Ca II $\lambda 3934$ absorptions in background stars like that done for several SNRs (e.g., Vela: Jenkins et al. 1976; Danks & Sembach 1995; Cha & Sembach 2000; IC 443: Welsh & Sallmen 2003; S147: Sallmen & Welsh 2004; Cygnus Loop: Fesen et al. 2019; W28: Ritchey 2020). Such observations might also help gauge the range of shock velocities across the very large and expansive remnants of G354-33 and Antlia.

We note that our finding that the G354-33 and Antlia nebula are both SNRs was a bit surprising. Out of the 300 or so confirmed SNRs, there are only about a dozen SNRs larger than two degrees and less than half that number located more than ten degrees off the Galactic plane (Green 2015, 2019). Now with the realization that some Galactic remnants can reach angular sizes several times larger than even Vela, it encourages the investigation of other large emission shells suspected as possible SNRs or previously viewed as unlikely SNR candidates. It also raises the value of SNR searches in the $|b| > 10^\circ$ range, generally viewed as unproductive.

Finally, we note that although far UV imaging appears to be a sensitive new tool for uncovering the presence of interstellar shocks, it is most useful in searching uncomplicated regions, like the objects discussed here located in the Galactic halo. However, the number of similar but unrecognized high latitude Galactic remnants is probably pretty small. Nonetheless, given the dozens of unconfirmed but seemingly likely or suspected SNRs in the literature (see list in Green 2019's catalogue), many new SNR discoveries may be aided by the use of UV imaging.

We thank Justin Rupert, Eric Galayda and the whole MDM staff for making the optical observations possible, and the SALT Observatory and Resident Astronomer staff for obtaining the excellent RSS spectra despite disruptions due to COVID-19 restrictions. We also thank R. Benjamin for helpful discussions. This work made use of the Simbad database, NASA's Skyview online data archives, and the Max Planck Institute for Radio Astronomy Survey Sampler. This work is part of R.A.F.'s Archangel III Research Program at Dartmouth. DM acknowledges support from the National Science Foundation from grants PHY-1914448 and AST-2037297.

REFERENCES

- Alikakos, J., Boumis, P., Christopoulou, P. E., & Goudis, C. D. 2012, *A&A*, 544, A140, doi: [10.1051/0004-6361/201219118](https://doi.org/10.1051/0004-6361/201219118)
- Aschenbach, B. 1998, *Nature*, 396, 141, doi: [10.1038/24103](https://doi.org/10.1038/24103)
- Bajaja, E., Cappa de Nicolau, C. E., Martin, M. C., et al. 1989, *A&AS*, 78, 345
- Bianchi, L. 2009, *Ap&SS*, 320, 11, doi: [10.1007/s10509-008-9761-3](https://doi.org/10.1007/s10509-008-9761-3)
- Blair, W. P., Kirshner, R. P., & Chevalier, R. A. 1981, *ApJ*, 247, 879, doi: [10.1086/159098](https://doi.org/10.1086/159098)
- Blondin, J. M., Wright, E. B., Borkowski, K. J., & Reynolds, S. P. 1998, *ApJ*, 500, 342, doi: [10.1086/305708](https://doi.org/10.1086/305708)

- Boumis, P., Mavromatakis, F., Paleologou, E. V., & Becker, W. 2002, *A&A*, 396, 225, doi: [10.1051/0004-6361:20021365](https://doi.org/10.1051/0004-6361:20021365)
- Boumis, P., Meaburn, J., López, J. A., et al. 2004, *A&A*, 424, 583, doi: [10.1051/0004-6361:20040410](https://doi.org/10.1051/0004-6361:20040410)
- Boumis, P., Xilouris, E. M., Alikakos, J., et al. 2009, *A&A*, 499, 789, doi: [10.1051/0004-6361/200811474](https://doi.org/10.1051/0004-6361/200811474)
- Bracco, A., Benjamin, R. A., Alves, M. I. R., et al. 2020, *A&A*, 636, L8, doi: [10.1051/0004-6361/202037975](https://doi.org/10.1051/0004-6361/202037975)
- Brandt, J. C., Roosen, R. G., Thompson, J., & Ludden, D. J. 1976, *ApJ*, 208, 109, doi: [10.1086/154585](https://doi.org/10.1086/154585)
- Brandt, J. C., Stecher, T. P., Crawford, D. L., & Maran, S. P. 1971, *ApJL*, 163, L99, doi: [10.1086/180676](https://doi.org/10.1086/180676)
- Cha, A. N., & Sembach, K. R. 2000, *ApJS*, 126, 399, doi: [10.1086/313306](https://doi.org/10.1086/313306)
- Chanot, A., & Sivan, J. P. 1983, *A&A*, 121, 19
- Chevalier, R. A. 1977, *ARA&A*, 15, 175, doi: [10.1146/annurev.aa.15.090177.001135](https://doi.org/10.1146/annurev.aa.15.090177.001135)
- Cioffi, D. F., McKee, C. F., & Bertschinger, E. 1988, *ApJ*, 334, 252, doi: [10.1086/166834](https://doi.org/10.1086/166834)
- Condon, J. J., Cotton, W. D., Greisen, E. W., et al. 1998, *AJ*, 115, 1693, doi: [10.1086/300337](https://doi.org/10.1086/300337)
- Cornett, R. H., Jenkins, E. B., Bohlin, R. C., et al. 1992, *ApJL*, 395, L9, doi: [10.1086/186476](https://doi.org/10.1086/186476)
- Cox, D. P., & Smith, B. W. 1974, *ApJL*, 189, L105, doi: [10.1086/181476](https://doi.org/10.1086/181476)
- Danks, A. C., & Sembach, K. R. 1995, *AJ*, 109, 2627, doi: [10.1086/117476](https://doi.org/10.1086/117476)
- Dopita, M. A., Binette, L., Dodorico, S., & Benvenuti, P. 1984, *ApJ*, 276, 653, doi: [10.1086/161653](https://doi.org/10.1086/161653)
- Downes, D. 1971, *AJ*, 76, 305, doi: [10.1086/111124](https://doi.org/10.1086/111124)
- Driessen, L. N., Domček, V., Vink, J., et al. 2018, *ApJ*, 860, 133, doi: [10.3847/1538-4357/aac32e](https://doi.org/10.3847/1538-4357/aac32e)
- Edelstein, J., Korpela, E. J., Adolfo, J., et al. 2006, *ApJL*, 644, L159, doi: [10.1086/505205](https://doi.org/10.1086/505205)
- Ferrand, G., & Safi-Harb, S. 2012, *Advances in Space Research*, 49, 1313, doi: [10.1016/j.asr.2012.02.004](https://doi.org/10.1016/j.asr.2012.02.004)
- Fesen, R. A., Blair, W. P., & Kirshner, R. P. 1985, *ApJ*, 292, 29, doi: [10.1086/163130](https://doi.org/10.1086/163130)
- Fesen, R. A., Neustadt, J. M. M., Black, C. S., & Koepfel, A. H. D. 2015, *ApJ*, 812, 37, doi: [10.1088/0004-637X/812/1/37](https://doi.org/10.1088/0004-637X/812/1/37)
- Fesen, R. A., Neustadt, J. M. M., How, T. G., & Black, C. S. 2019, *MNRAS*, 486, 4701, doi: [10.1093/mnras/stz1140](https://doi.org/10.1093/mnras/stz1140)
- Fesen, R. A., Weil, K. E., Raymond, J. C., et al. 2020, *MNRAS*, 498, 5194, doi: [10.1093/mnras/staa2765](https://doi.org/10.1093/mnras/staa2765)
- Finkbeiner, D. P. 2003, *ApJS*, 146, 407, doi: [10.1086/374411](https://doi.org/10.1086/374411)
- Gaustad, J. E., McCullough, P. R., Rosing, W., & Van Buren, D. 2001, *PASP*, 113, 1326, doi: [10.1086/323969](https://doi.org/10.1086/323969)
- Green, D. A. 1984, *MNRAS*, 209, 449, doi: [10.1093/mnras/209.3.449](https://doi.org/10.1093/mnras/209.3.449)
- . 2004, *Bulletin of the Astronomical Society of India*, 32, 335. <https://arxiv.org/abs/astro-ph/0411083>
- . 2015, *MNRAS*, 454, 1517, doi: [10.1093/mnras/stv1885](https://doi.org/10.1093/mnras/stv1885)
- . 2019, *Journal of Astrophysics and Astronomy*, 40, 36, doi: [10.1007/s12036-019-9601-6](https://doi.org/10.1007/s12036-019-9601-6)
- Gull, T. R., Kirshner, R. P., & Parker, R. A. R. 1977, *ApJL*, 215, L69, doi: [10.1086/182480](https://doi.org/10.1086/182480)
- Gum, C. S. 1952, *The Observatory*, 72, 151
- . 1955, *MmRAS*, 67, 155
- Hartigan, P., Raymond, J., & Hartmann, L. 1987, *ApJ*, 316, 323, doi: [10.1086/165204](https://doi.org/10.1086/165204)
- Haslam, C. G. T., Klein, U., Salter, C. J., et al. 1981, *A&A*, 100, 209
- Haslam, C. G. T., Salter, C. J., Stoffel, H., & Wilson, W. E. 1982, *A&AS*, 47, 1
- How, T. G., Fesen, R. A., Neustadt, J. M. M., Black, C. S., & Outters, N. 2018, *MNRAS*, 478, 1987, doi: [10.1093/mnras/sty1007](https://doi.org/10.1093/mnras/sty1007)
- Howarth, I. D., & van Leeuwen, F. 2019, *MNRAS*, 484, 5350, doi: [10.1093/mnras/stz291](https://doi.org/10.1093/mnras/stz291)
- Howell, D. A. 2017, *Superluminous Supernovae*, ed. A. W. Alsabti & P. Murdin, 431, doi: [10.1007/978-3-319-21846-5_41](https://doi.org/10.1007/978-3-319-21846-5_41)
- Iacobelli, M., Burkhart, B., Haverkorn, M., et al. 2014, *A&A*, 566, A5, doi: [10.1051/0004-6361/201322982](https://doi.org/10.1051/0004-6361/201322982)
- Jenkins, E. B., Silk, J., & Wallerstein, G. 1976, *ApJS*, 32, 681, doi: [10.1086/190412](https://doi.org/10.1086/190412)
- Kim, I. J., Seon, K. I., Min, K. W., et al. 2010, *ApJ*, 722, 388, doi: [10.1088/0004-637X/722/1/388](https://doi.org/10.1088/0004-637X/722/1/388)
- Kopsacheili, M., Zezas, A., & Leonidaki, I. 2020, *MNRAS*, 491, 889, doi: [10.1093/mnras/stz2594](https://doi.org/10.1093/mnras/stz2594)
- Kregenow, J., Edelstein, J., Korpela, E. J., et al. 2006, *ApJL*, 644, L167, doi: [10.1086/505196](https://doi.org/10.1086/505196)
- Leonidaki, I., Boumis, P., & Zezas, A. 2013, *MNRAS*, 429, 189, doi: [10.1093/mnras/sts324](https://doi.org/10.1093/mnras/sts324)
- Long, K. S. 2017, *Galactic and Extragalactic Samples of Supernova Remnants: How They Are Identified and What They Tell Us*, ed. A. W. Alsabti & P. Murdin, 2005, doi: [10.1007/978-3-319-21846-5_90](https://doi.org/10.1007/978-3-319-21846-5_90)
- Maggi, P., Haberl, F., Kavanagh, P. J., et al. 2014, *A&A*, 561, A76, doi: [10.1051/0004-6361/201322820](https://doi.org/10.1051/0004-6361/201322820)
- Martini, P., Stoll, R., Derwent, M. A., et al. 2011, *PASP*, 123, 187, doi: [10.1086/658357](https://doi.org/10.1086/658357)
- Massey, P., & Gronwall, C. 1990, *ApJ*, 358, 344, doi: [10.1086/168991](https://doi.org/10.1086/168991)
- McCullough, P. R., & Benjamin, R. A. 2001, *AJ*, 122, 1500, doi: [10.1086/322097](https://doi.org/10.1086/322097)

- McCullough, P. R., Fields, B. D., & Pavlidou, V. 2002, *ApJL*, 576, L41, doi: [10.1086/343100](https://doi.org/10.1086/343100)
- McKee, C. F., & Ostriker, J. P. 1977, *ApJ*, 218, 148, doi: [10.1086/155667](https://doi.org/10.1086/155667)
- Neustadt, J. M. M., Fesen, R. A., & Black, C. S. 2017, *MNRAS*, 469, 516, doi: [10.1093/mnras/stx867](https://doi.org/10.1093/mnras/stx867)
- Nishikida, K., Edelstein, J., Korpela, E. J., et al. 2006, *ApJL*, 644, L171, doi: [10.1086/505197](https://doi.org/10.1086/505197)
- Oke, J. B. 1974, *ApJS*, 27, 21, doi: [10.1086/190287](https://doi.org/10.1086/190287)
- Osterbrock, D. E., & Ferland, G. J. 2006, *Astrophysics of gaseous nebulae and active galactic nuclei*
- Penprase, B. E., & Blades, J. C. 1992, *ApJ*, 391, 276, doi: [10.1086/171343](https://doi.org/10.1086/171343)
- Pfeffermann, E., & Aschenbach, B. 1996, in *Roentgenstrahlung from the Universe*, ed. H. U. Zimmermann, J. Trümper, & H. Yorke, 267–268
- Predehl, P., Sunyaev, R. A., Becker, W., et al. 2020, *Nature*, 588, 227, doi: [10.1038/s41586-020-2979-0](https://doi.org/10.1038/s41586-020-2979-0)
- Purcell, C. R., Gaensler, B. M., Sun, X. H., et al. 2015, *ApJ*, 804, 22, doi: [10.1088/0004-637X/804/1/22](https://doi.org/10.1088/0004-637X/804/1/22)
- Raymond, J. C., Caldwell, N., Fesen, R. A., et al. 2020, *ApJ*, 888, 90, doi: [10.3847/1538-4357/ab5e84](https://doi.org/10.3847/1538-4357/ab5e84)
- Reich, W. 1982, *A&AS*, 48, 219
- Reich, W., & Reich, P. 2009, in *Cosmic Magnetic Fields: From Planets, to Stars and Galaxies*, ed. K. G. Strassmeier, A. G. Kosovichev, & J. E. Beckman, Vol. 259, 603–612, doi: [10.1017/S1743921309031433](https://doi.org/10.1017/S1743921309031433)
- Ritchey, A. M. 2020, *MNRAS*, 495, 2909, doi: [10.1093/mnras/staa1375](https://doi.org/10.1093/mnras/staa1375)
- Sabin, L., Parker, Q. A., Contreras, M. E., et al. 2013, *MNRAS*, 431, 279, doi: [10.1093/mnras/stt160](https://doi.org/10.1093/mnras/stt160)
- Sallmen, S., & Welsh, B. Y. 2004, *A&A*, 426, 555, doi: [10.1051/0004-6361:20040093](https://doi.org/10.1051/0004-6361:20040093)
- Seon, K. I., Han, W., Nam, U. W., et al. 2006, *ApJL*, 644, L175, doi: [10.1086/505201](https://doi.org/10.1086/505201)
- Shelton, R. L. 1998, *ApJ*, 504, 785, doi: [10.1086/306107](https://doi.org/10.1086/306107)
- Shinn, J. H., Min, K. W., Lee, C. N., et al. 2006, *ApJL*, 644, L189, doi: [10.1086/505263](https://doi.org/10.1086/505263)
- Shinn, J.-H., Min, K. W., Sankrit, R., et al. 2007, *ApJ*, 670, 1132, doi: [10.1086/522219](https://doi.org/10.1086/522219)
- Sivan, J. P. 1974, *A&AS*, 16, 163
- Stupar, M., & Parker, Q. A. 2011, *MNRAS*, 414, 2282, doi: [10.1111/j.1365-2966.2011.18547.x](https://doi.org/10.1111/j.1365-2966.2011.18547.x)
- . 2012, *MNRAS*, 419, 1413, doi: [10.1111/j.1365-2966.2011.19797.x](https://doi.org/10.1111/j.1365-2966.2011.19797.x)
- Stupar, M., Parker, Q. A., & Filipović, M. D. 2008, *MNRAS*, 390, 1037, doi: [10.1111/j.1365-2966.2008.13761.x](https://doi.org/10.1111/j.1365-2966.2008.13761.x)
- Stupar, M., Parker, Q. A., Filipović, M. D., et al. 2007, *MNRAS*, 381, 377, doi: [10.1111/j.1365-2966.2007.12296.x](https://doi.org/10.1111/j.1365-2966.2007.12296.x)
- Stupar, M., Parker, Q. A., & Frew, D. J. 2018, *MNRAS*, 479, 4432, doi: [10.1093/mnras/sty1684](https://doi.org/10.1093/mnras/sty1684)
- Sutherland, R. S., & Dopita, M. A. 2017, *ApJS*, 229, 34, doi: [10.3847/1538-4365/aa6541](https://doi.org/10.3847/1538-4365/aa6541)
- Testori, J. C., Reich, P., Bava, J. A., et al. 2001, *A&A*, 368, 1123, doi: [10.1051/0004-6361:20010088](https://doi.org/10.1051/0004-6361:20010088)
- Testori, J. C., Reich, P., & Reich, W. 2008, *A&A*, 484, 733, doi: [10.1051/0004-6361:20078842](https://doi.org/10.1051/0004-6361:20078842)
- van Dokkum, P. G. 2001, *PASP*, 113, 1420, doi: [10.1086/323894](https://doi.org/10.1086/323894)
- Welsh, B. Y., & Sallmen, S. 2003, *A&A*, 408, 545, doi: [10.1051/0004-6361:20030908](https://doi.org/10.1051/0004-6361:20030908)
- Woermann, B., Gaylard, M. J., & Otrupcek, R. 2001, *MNRAS*, 325, 1213, doi: [10.1046/j.1365-8711.2001.04558.x](https://doi.org/10.1046/j.1365-8711.2001.04558.x)